United States
Environmental Protection
Agency

Office of
Research and Development
Washington, DC 20460

EPA/600/R-92/143
August 1992

EPA

Acoustic Location of Leaks in Pressurized Underground Petroleum Pipelines

EPA/600/R-92/143
August 1992

ACOUSTIC LOCATION OF LEAKS IN PRESSURIZED UNDERGROUND PETROLEUM PIPELINES

by

Eric G. Eckert and Joseph W. Maresca, Jr.
Vista Research, Inc.
Mountain View, California 94042

Contract No. 68-03-3409

Project Officer

Robert W. Hillger
Superfund Technology Demonstration Division
Risk Reduction Engineering Laboratory
Edison, New Jersey 08837

RISK REDUCTION ENGINEERING LABORATORY
OFFICE OF RESEARCH AND DEVELOPMENT
U.S. ENVIRONMENTAL PROTECTION AGENCY
CINCINNATI, OHIO 45268

DISCLAIMER

This material has been funded wholly or in part by the United States Environmental Protection Agency under Contract 68-03-3409 to CDM Federal Programs Corporation. It has been subject to the Agency's peer and administrative review, and it has been approved for publication as an EPA document. Mention of trade names or commercial products does not constitute endorsement or recommendation for use.

FOREWORD

Today's rapidly developing and changing technologies and industrial products frequently carry with them the increased generation of materials that, if improperly dealt with, can threaten both public health and the environment. The U. S. Environmental Protection Agency is charged by Congress with protecting the nation's land, air, and water resources. Under a mandate of national environmental laws, the agency strives to formulate and implement actions leading to a compatible balance between human activities and the ability of natural systems to support and nurture life. These laws direct the EPA to perform research to define our environmental problems, measure the impacts, and search for solutions.

The Risk Reduction Engineering Laboratory is responsible for planning, implementing, and managing research, development, and demonstration programs to provide an authoritative, defensible engineering basis in support of the policies, programs, and regulations of the EPA with respect to drinking water, wastewater, pesticides, toxic substances, solid and hazardous wastes, and Superfund-related activities. This publication is one of the products of that research and provides a vital communication link between the researcher and the user community.

The work reported in this document has application to the remediation of leaks from underground pressurized pipelines containing petroleum or other hazardous chemicals.

E. Timothy Oppelt, Director
Risk Reduction Engineering Laboratory

ABSTRACT

Experiments were conducted at the UST Test Apparatus Pipeline in which three acoustic sensors separated by a maximum distance of 38.1 m (125 ft) were used to monitor signals produced by 11.4-, 5.7-, and 3.8-L/h (3.0-, 1.5-, and 1.0-gal/h) leaks in the wall of a 5-cm- (2-in.-) diameter pressurized petroleum pipeline. The line pressures and hole diameters used in the experiments ranged from 69 to 138 kPa (10 to 20 psi) and 0.4 to 0.7 mm (0.01 to .03 in.), respectively. Application of a leak location algorithm based upon the technique of coherence function analysis resulted in mean differences between predicted and actual leak locations of approximately 10 cm. The standard deviations of the location estimates were approximately 30 cm. This is a significant improvement (i.e., smaller leaks over longer distances) over the cross-correlation-based techniques which are currently being used.

Spectra computed from leak-on and leak-off time series indicate that the majority of acoustic energy received in the far field of the leak is concentrated in a frequency band from 1 to 4 kHz. The strength of the signal within this band was found to be proportional to the leak flow rate and line pressure. Energy propagation from leak to sensor was observed via three types of wave motion: longitudinal waves in the product, and longitudinal and transverse waves in the steel. The similarity between the measured wave speed and the nominal speed of sound in gasoline suggests that longitudinal waves in the product dominate the spectrum of received acoustic energy. The effects of multiple-mode wave propagation and the reflection of acoustic signals within the pipeline were observed as non-random fluctuations in the measured phase difference between sensor pairs.

Additional experiments with smaller holes and higher pressures (138 to 345 kPa [20 to 50 psi]) are required to determine the smallest leaks that can be located over distances of several hundred feet. The current experiments indicate that improved phase-unwrapping algorithms and/or lower noise instrumentation are required to optimize system performance.

This report was submitted in fulfillment of Contract No. 68-03-3409 by Vista Research, Inc., under the sponsorship of the U.S. Environmental Protection Agency. This report covers a period from 23 January 1991 to 31 October 1991, and work was completed as of 30 September 1991.

TABLE OF CONTENTS

LIST OF FIGURES

LIST OF TABLES

LIST OF ABBREVIATIONS

cm	=	Centimeters
dB	=	Decibels
°	=	Degrees
< >	=	Expectation value or average value
f	=	Frequency
ft	=	Feet
γ^2	=	Squared complex coherence function
gal	=	Gallons
h	=	Hours
Hz	=	Hertz
in.	=	Inches
k	=	Wavenumber
kHz	=	Kilohertz
kPa	=	Kilopascals
L	=	Liters
m	=	Meters
mm	=	Millimeters
m (t)	=	Measured quantity (time domain)
M (f)	=	Measured quantity (frequency domain)
P	=	Pressure; level of statistical significance
P_D	=	Probability of detection
P_{FA}	=	Probability of false alarm
ϕ	=	Phase angle
π	=	Pi
psi	=	Pounds per square inch
ρ_{xy}	=	Normalized cross-correlation coefficient
s	=	Seconds
σ	=	Standard deviation
SNR	=	Signal-to-noise ratio
t	=	Time
τ	=	Time
v	=	Wave speed
x	=	Measurement of distance

EPA	=	Environmental Protection Agency
RREL	=	Risk Reduction Engineering Laboratory
UST(s)	=	Underground Storage Tank(s)

ACKNOWLEDGMENTS

This research report for evaluating the feasibility of locating small leaks in undergound pressurized pipelines containing petroluem and other hazardous liquids by means of a passive acoustic sensing system was prepared for the U.S. Environmental Protection Agency's (EPA's) Risk Reduction Engineering Laboratory (RREL) on Contract No. 68-03-3409. Robert W. Hillger and James J. Yezzi were the Technical Program Monitors on the Work Assignment for EPA/RREL. Technical review was provided by Messrs. Hillger and Yezzi and by Anthony N. Tafuri, Section Chief, Underground Storage Tank Program. The authors would especially like to acknowledge CTI, Inc., for the loan of the acoustic sensing equipment used in the experiments. This document was edited by Monique Seibel and prepared for publication by Pamela Webster and Christine Lawson.

SECTION 1

INTRODUCTION

Underground pressurized pipelines are frequently used to transfer liquid products for many industrial applications. Some of these pipelines are associated with the underground storage tanks typically found at retail stations, and others with tanks at industrial storage facilities; they can contain petroleum products or a variety of other chemicals. There are many systems that can be used to detect leaks in underground pressurized pipelines. These leak detection systems are designed for use on pipelines that are typically 5 cm (2 in.) in diameter and generally 15.2 to 61.0 m (50 to 200 ft) in length. The EPA regulations [1] require that the leak detection equipment used to test a pipeline monthly be capable of detecting leaks at least as small as 0.76 L/h (0.2 gal/h) with a probability of detection (P_D) of 95% and a probability of false alarm (P_{FA}) of 5%. If the equipment is used to test the line annually, it must be able to detect leaks as small as 0.38 L/h (0.1 gal/h); in the regulations, this type of test is designated as a line tightness test.

If a leak is found, remediation must follow. The first step in any remediation is to find the location of the leak. At the present time, there are two methods being used, but neither method is totally acceptable. The first method is to systematically uncover the line and perform a visual inspection for leaks. While this method works, it is time consuming, disruptive to operations, and costly. In addition, the line is subject to damage during the excavation process. The second method is to use a helium- or halogen-tracer technique, but both tracer techniques have operational and accuracy problems. There is a need for a nondestructive method of leak location that is accurate, relatively simple to use, and applicable to a wide variety of pipelines and pipeline products.

One method of expediting the remediation process is the application of remote sensing techniques to the pipeline in order to accurately locate the leak. Passive-acoustic measurements, combined with advanced signal-processing methods, may provide a means by which to locate small leaks in limited-access pipeline delivery systems. The concept of using passive acoustics to determine the spatial location of leaks has been around for some time, but this approach has not been applied to underground petroleum pipelines. While it is known that a pressurized underground pipeline that is leaking emits an acoustic signal, the strength and characteristics of the signal associated with the leak are not well known.

Acoustic systems have been successfully used to detect and locate leaks in nuclear reactors for many years [2]. By means of a cross-correlation analysis, 100- to 400-kHz acoustic sensors spaced at 5- to 10-m intervals can be used to detect leaks of about 3.8 L/min (1 gal/min) with an accuracy that is within 0.5 m. A similar approach has been tested for locating water leaks in 10- to 25-cm- (4- to 10-in.-) diameter underground district heating and cooling pipes [3]. Theoretical predictions based on Kupperman et al. [3] suggest that leaks of 7.6 L/min (2 gal/min) could be pinpointed to within several meters with sensors spaced at several hundred meters. Using monitoring frequencies less than 25 kHz makes this wider spacing possible; frequencies between 1 and 5 kHz appear to give the best results. In the program of experiments conducted in Kupperman et al. [3], the sensors were externally mounted to the steel pipe. Interestingly, leaks that occurred in a steel pipe covered with insulation material (urethane and a rubber jacket) showed a higher level of signal intensity than leaks that occurred in an uncovered pipe. This suggests that if a pipeline is located underground rather than above ground, the surrounding backfill and soil may enhance the acoustic leak signal. The predictions were based upon models that were validated using a 25.9-m- (85-ft-) long, 7.6-cm- (3-in.-) diameter aboveground pipeline that contained water and in which leaks of 5.7 L/min (1.5 gal/min) were induced at a pressure of 827 kPa (120 psi). Field tests on an operational line were also done.

Figure 1.1 shows a simple representation of a passive-acoustic leak location system in which a pair of transducers bracketing a leak simultaneously sample the acoustic signal. The leak emits an acoustic wave, which propagates down a pressurized pipeline, and is received at the two transducers. A microcomputer system acquires and analyzes the data needed to find the location of the leak. The data are converted from an analog signal to a digital signal with an A/D converter. These time series, recorded by spatially separated sensors, then serve as input to a leak location algorithm.

Cross-correlation analysis works well provided that the signal is very strong or that the background noise is not excessive. When the acoustic signal is weak in relation to the level of background noise or has a finite frequency bandwidth, more sophisticated signal processing techniques are available. Advanced signal processing is required if any of the following objectives are to be achieved: (1) detection of leaks smaller than several gallons per hour, (2) a reduction in the number of false alarms and missed detections due to operational or ambient noise, and (3) an increase in the distance between sensors bracketing the leak. One such technique is *coherence function analysis.*

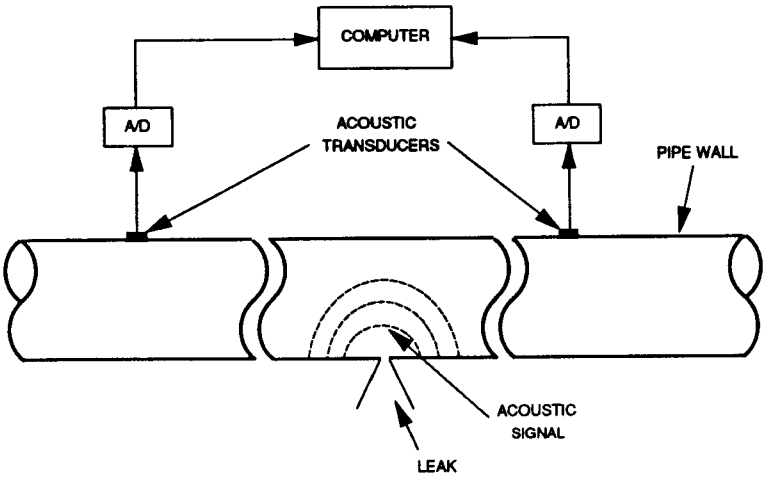

Figure 1.1. Example of a passive-acoustic leak location system.

The application of coherence function analysis to signals measured by two or more transducers is the means by which the source of the signal is best located. Coherence function analysis, which estimates the correspondence between two measurements as a function of frequency, is analogous to the squared correlation coefficient, but is a *far more powerful tool* in signal estimation and location. The coherence magnitude measures the strength of the correspondence, and the coherence phase measures the relative time delay. In contrast, the correlation coefficient is a measure of correspondence that is the result of an integration over all frequencies. If the correspondence is frequency-dependent, or if the phase dependence of the correspondence is a nonlinear function of frequency, the correlation is degraded. By contrast, coherence is a direct measure of the complex frequency correspondence between two measurements, and, therefore, preserves the actual correspondence between the two measurements of the signal.

In the last five to ten years there have been significant advances in commercially available acoustic sensors, in powerful computers that are both small and inexpensive, and in digital signal processing. This means that acoustic leak location can be made available in a portable package, a possibility that makes it an attractive and viable option. Acoustic systems are attractive from an operational standpoint because the test is short (a few minutes) and the sensors can be mounted directly on the outside of the pipeline. Acoustic systems have direct application to the 15.2- to 61.0-m (50- to 200-ft) pipelines found at retail service stations because the sensors can be placed at each end of the line. Acoustic systems are also applicable to longer pipelines, but access at several points along the line must be provided.

The objective of this work was to make an estimate of the accuracy of locating a leak in a pressurized petroleum pipeline, by means of passive acoustic sensors mounted on the outside wall of the pipeline, as a function of leak rate and distance between acoustic sensors. While there are regulatory standards for detection of leaks in underground pressurized pipelines, there are no standards for leak location. For rapid remediation, it would be highly desirable if the leak could be located within 10% of the length of the pipeline in the case of a line longer than 30.5 m (100 ft), or within 3.0 m (10 ft) in the case of a line shorter than 30.5 m (100 ft). This limits the excavation to only a small fraction of the line. As will be shown below, theoretical estimates suggest that the accuracy of the proposed technique should be better than 25 cm. These theoretical estimates, however, assume that the leak signal is large compared to the noise.

It would be desirable if the acoustic system could locate leaks as small as the detection standards in EPA's regulations (i.e., either 0.38 or 0.76 L/h [0.1 or 0.2 gal/h]). However, the system can be useful nonetheless, even if it does not meet these standards, since many of the leaks actually detected are much larger. One to two drops of liquid per second produces leaks as large as 0.38 L/h (0.1 gal/h); such a leak might occur if, for example, the threaded connection between two pipes or between a pipe and another appurtenance is not tight. Any type of small hole in the pipeline system will produce a large leak. A 0.08-cm- (1/32-in.-) diameter hole in a pipeline pressurized to 138 kPa (20 psi) would, for example, result in a flow rate of approximately 19 L/h (5.0 gal/h). Leaks of this magnitude should be large enough to locate with an acoustic system providing that the length of the line is not too long.

The results of this work are described below and are summarized in a peer-reviewed journal article being published by the American Society for Testing and Materials [4].

SECTION 2

CONCLUSIONS

Passive acoustic measurements, combined with advanced signal processing techniques based on coherence analysis, offer a promising method for the location of small leaks in pressurized petroleum pipelines found at retail service stations and industrial storage facilities. While the results presented in this work represent a significant improvement over previous pipeline leak location efforts, additional research and development are required in order to optimize system performance. Location of leaks of several tenths of a gallon per hour over distances of several hundred feet should ultimately be possible.

Experiments were conducted on a pipeline at the UST Test Apparatus in which three acoustic sensors separated by a maximum distance of 38 m (125 ft) were used to monitor signals produced by 3.8-, 5.7-, and 11.4-L/h (1.0-, 1.5-, and 3.0-gal/h) gasoline leaks. These flow rates were generated through drilled holes 0.4 to 0.7 mm (0.01 to 0.03 in.) in diameter. The three-transducer system enabled the propagation speed of acoustic waves to be measured for particular combinations of product, pipeline geometry, and analysis frequency band. Data recorded at the higher flow rates (5.7 and 11.4 L/h [1.5 and 3.0 gal/h]) correspond to full line pressure (103 to 138 kPa [15 to 20 psi]), while data recorded at the lower flow rate (3.8 L/h [1.0 gal/h]) were obtained under partial line pressure (69 kPa [10 psi]) due to the limitation imposed by the minimum available hole diameter (0.4 mm [0.01 in.]). Application of a leak location algorithm based upon the technique of coherence function analysis resulted in mean differences between predicted and actual leak locations of 8.7 cm (11.4 L/h [3.0 gal/h]), 3.6 cm (5.7 L/h [1.5 gal/h]), and -11.6 cm (3.8 L/h [1.0 gal/h]). Standard deviations of the location estimates were 26.1 cm (11.4 L/h [3.0 gal/h]), 26.3 cm (5.7 L/h [1.5 gal/h]), and 39.1 cm (3.8 L/h [1.0 gal/h]). The mean propagation speed was 915 m/s with a standard deviation of 146 m/s.

Data recorded in the presence of a 1.9-L/h (0.5-gal/h) leak were obtained as part of an investigation of signal strength as a function of line pressure for a fixed-diameter hole (0.4 mm [0.01 in.]). The 1.9-L/h (0.5-gal/h) leak produced a detectable signal; however, because of the reduced line pressure, the algorithm, as applied, yielded no location estimates.

Spectra computed from leak-on and leak-off time series indicate that the majority of acoustic energy received in the far field of the leak is concentrated in a frequency band from 1 to 4 kHz. The strength of the acoustic signal within this band was observed to be proportional to the leak flow rate and line pressure, as expected. Energy propagation from leak to sensor was

observed via three forms of wave motion: longitudinal waves in the product, and both transverse and longitudinal waves in the steel. Isolation of each of these propagation modes was achieved through the use of gasoline and CO_2 as the product fluids, and through the generation of impulsive calibration signals. Though each of these propagation modes is believed to contribute to the overall received signal, longitudinal wave motion in the product was clearly the dominant propagation mode for liquid-filled pipelines. The effects of multiple-mode wave propagation and the reflection of acoustic signals within the pipeline were observed as non-random fluctuations in the measured phase difference between sensor pairs.

Accurate leak location requires the identification of frequency bands within which a high degree of similarity is maintained between acoustic signals propagated along different paths from leak to sensor. Coherence function analysis provides the best means of gauging this similarity, and thus separating useful information concerning the leak location from ambient or system noise. While the signal-to-noise ratio (SNR) was observed to be generally high within the entire 1- to 4-kHz frequency band, continuous regions of high coherence appropriate for source location were typically 100 to 500 Hz in width. Several data sets recorded in the presence of the 11.4-L/h (3-gal/h) leak exhibited high coherence over a 2-kHz bandwidth. Location estimates obtained by means of the cross-correlation technique showed that without the detailed knowledge of signal similarity provided by the coherence function, cross-correlation analysis cannot locate small leaks with acceptable accuracy. The observed correspondence between measured and predicted phase shifts within the 1- to 4-kHz frequency band demonstrates the need to develop a more sophisticated location algorithm such that a greater fraction of the information contained in coherent leak signals may be processed.

Buried pipelines provide a generally quiet ambient environment in which to perform acoustic measurements. Since the SNR for a given leak largely determines the ability of a passive acoustic system to locate the leak, the system noise level should be determined by ambient acoustic noise, rather than electronic noise. The combination of sensors (CTI-30s) and preamplifiers (Panametrics 5660-Cs) used in this work was incapable of resolving the low levels of ambient acoustic noise associated with the pipeline at the UST Test Apparatus. Improved system performance may be attained through the use of transducers with greater sensitivity in the low frequency range (1 to 10 kHz) and low-noise preamplifiers.

SECTION 3

RECOMMENDATIONS

The full capability of the location algorithm was not evaluated in these tests. The smallest hole used to generate a leak in the experiments was 0.4 mm (0.01 in.). At a line pressure of 138 kPa (20 psi) this resulted in a leak rate of 3.8 L/h (1.0 gal/h). It is recommended that additional experiments be performed with smaller holes at higher line pressures (138 to 345 kPa [20 to 50 psi]) to determine the minimum leak rate that can be reliably located. The current work indicates that further improvement can be realized through the application of better phase-unwrapping algorithms and better instrumentation. A better understanding of the underlying physics of pipeline acoustics, including the propagation modes and source mechanisms of the acoustic leak signal, will help optimize the algorithms and the hardware. It is recommended that the following work be performed to extend the technology:

- development of a location algorithm capable of processing the coherence phase over an arbitrarily wide frequency band
- characterization of the wave propagation modes excited by the acoustic leak signal and the degree to which each mode enhances or degrades the leak location estimate
- reduction of system noise through transducers specifically designed for low-frequency, high-sensitivity applications, and through the use of low-noise, audio-range preamplifiers
- automation of the data acquisition system and signal processing algorithm, and evaluation of system performance on a variety of actual pipelines

SECTION 4

LOCATION OF A CONTINUOUS LEAK SIGNAL

The primary function of the location algorithm is to estimate the time delay between acoustic leak signals received by a pair of sensors. The time delay, which is estimated from phase measurements made in the frequency domain for continuous leak signals, can be used to estimate the source location (for sensors bracketing the leak) or the propagation speed of the acoustic waves (for non-bracketing sensor pairs). Two criteria must be satisfied in order that accurate location estimates result from the application of the location algorithm: (1) the received signals must originate primarily at a single, localized source and propagate as plane waves along (or within) the pipeline, and (2) the received signals must maintain a reasonable degree of similarity over the maximum sensor separation. If criterion (1) is satisfied, the difference in phase between received waves of a given frequency is simply related to the time delay between signals that arrive at the different sensor locations. The accuracy with which the time delays can be measured is related to criterion (2). The similarity between signals emitted from a localized source and received at separate locations is determined by the signal strength relative to ambient noise (i.e., the signal-to-noise ratio) and the difference in propagation path between the source and each sensor. Due to the complex manner in which the acoustic leak signal is produced (turbulent flow and cavitation) and the many variations in the propagation medium (valves, branches, reflective ends), the degree of signal similarity is not uniform over a broad range of frequencies. Though the signal-to-noise ratio provides a reasonable estimate of the frequency band for which accurate leak locations may be obtained, a more sensitive measure of signal similarity is required for the location of small leaks (e.g., 11.4 L/h [3 gal/h] or less).

The proposed detection algorithm is designed to locate leaks with a high signal-to-noise ratio[1]. As the leak becomes smaller or the line becomes longer, the SNR will eventually become small enough that routine location estimates cannot be made. The accuracy of the location estimate depends on the estimate of the sound speed, the resolution of the data acquisition system, the strength of the signal compared to the noise, and the signal processing algorithm. The experimental uncertainty in locating a leak can be estimated from the standard deviation of the location estimates made from many realizations of the measurement of the leak for one or more

1 The signal-to-noise ratio is estimated from the ratio of the received power at the output of the measurement system over a specified frequency band while a signal is present, divided by the output power measured at the receiver over the same frequency band while a signal is not present.

leak rates and at one or more separation distances of the sensors bracketing the leak. The algorithms proposed for leak location and the estimates of the uncertainty in applying these algorithms are described below.

4.1 Location Algorithm

Consider two measurements of the signal, $m_1(t)$ and $m_2(t)$, where each represents the sum of a desired signal, s(t), and a contaminating noise component, n(t). The signal, s(t), would be the acoustic signal emanating from the leaking pipeline, and the contaminating noise component, n(t), could be ambient noise in the measurement environment that is uncorrelated at the separated acoustic sensors. The coherence function, $\gamma^2(f)$, is the normalized cross spectrum of the two measurements,

$$\gamma^2(f) = \frac{\overline{M_1(f)M_2^*(f)}}{\sqrt{\overline{|M_1(f)|^2}}\sqrt{\overline{|M_2(f)|^2}}}, \tag{4.1}$$

where upper-case letters denote the Fourier transform of the respective quantities and the overbar denotes the ensemble average. As noted above, the coherence is complex and the phase, $\phi(f)$, measures the relative time delay between the two signals at a given frequency f. The coherence function ranges in magnitude from 0 (signals completely uncorrelated) to 1 (signals completely correlated). Values of $\gamma^2(f)$ exceeding 95% of the noise fluctuations are usually taken as indicating a reliable phase measurement.

If the acoustic leak signal is approximated as a collection of propagating acoustic plane waves that obey the simple linear dispersion relation

$$2\pi f = kV, \tag{4.2}$$

where k is the wavenumber and V is the propagation speed, the differential separation between two sensors, Δx, and the frequency-dependent phase, $\phi(f)$, are simply related by

$$\phi(f) = 2\pi f\left(\frac{\Delta x}{V}\right). \tag{4.3}$$

Through the use of coherence function analysis, it is possible to isolate portions of the acoustic spectrum within which the linear dispersion relation is obeyed. The measured phase shift, $\phi(f)$, within these frequency bands can then be used to estimate either the propagation speed of acoustic waves or the differential sensor separation. Because the coherence phase is confined to the range $-180° \leq \phi \leq 180°$, the measured phase generally differs from the actual phase by an unknown factor of 360°, except at very low frequencies and/or very small sensor

separations. As a consequence, the measured phase cannot be accurately unwrapped except within frequency bands where $\gamma^2(f)$ is high; thus, a differential form of Eq. (4.3) must be used to relate sensor separation, propagation speed, and coherence phase:

$$\frac{d\phi}{df} = \frac{2\pi\Delta x}{V}, \tag{4.4}$$

in which, for the sake of simplicity, it is assumed that the medium is nondispersive.

The three-sensor approach illustrated in Figure 4.1 was used to locate leaks in an underground pipeline. This configuration is similar to the one shown in Figure 1.1, except that sensor pair B-C is used to measure the *in situ* wave speed, while sensor pairs A-B or A-C are used to estimate the leak location. Knowledge of the wave speed improves the accuracy of the leak location estimate. However, the wave speed associated with a particular product and pipeline geometry is usually unknown. Therefore, it is useful to make an experimental estimate of the wave speed.

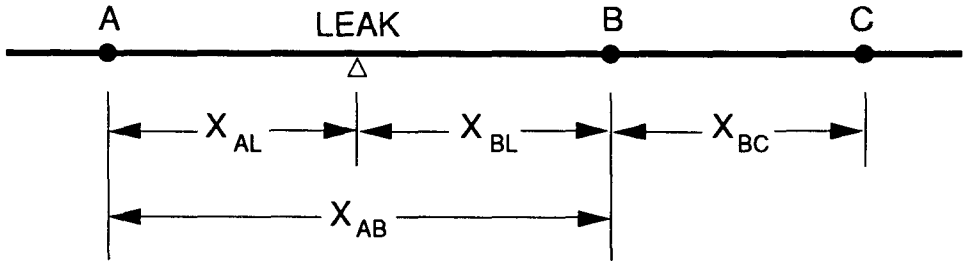

Figure 4.1. Three-sensor approach to acoustic location of leaks.

Application of Eq. (4.4) to sensors A and B, which bracket the leak, yields a simple relationship between measured phase, wave speed, and leak location:

$$X_{AL} = \frac{X_{AB}}{2} - \frac{V}{4\pi}\frac{d\phi_{AB}}{df} \tag{4.5}$$

$$X_{BL} = \frac{X_{AB}}{2} + \frac{V}{4\pi}\frac{d\phi_{AB}}{df} \tag{4.6}$$

where L denotes the location of the leak. The wave speed is estimated from the measured phase between sensors B and C:

$$V = 2\pi X_{BC}\left[\frac{d\phi_{BC}}{df}\right]^{-1}. \tag{4.7}$$

4.2 Location Errors

The coherence phase required for the estimation of the leak location and wave speed is most accurately measured (i.e., has a low probability of being a noise fluctuation) when the coherence amplitude, $\gamma^2(f)$, is significantly above the noise. The value of the coherence amplitude associated with a level of statistical significance, P, is given by

$$\gamma_P^2 = 1-(1-P)^{\beta}, \quad \beta = \frac{1}{0.5(n+1)-1} \tag{4.8}$$

where n is the number of independent data segments used to compute $\gamma^2(f)$. If P is 0.95 and n is 15, then for any value $\gamma^2(f)$ greater than 0.35, there is less than a 0.05 (5%) chance that $\gamma^2(f)$ was produced by a noise fluctuation.

An estimate of the one-standard-deviation uncertainty in the phase measurements, $\sigma\{\phi_{AB}(f)\}$, derived from coherence measurements between any two sensors (e.g., A and B) is given by

$$\sigma\{\phi_{AB}(f)\} = \frac{[1-\gamma_{AB}(f)^2]^{1/2}}{\gamma_{AB}\sqrt{2n}} \tag{4.9}$$

by Bendat and Piersol [5]. Eq. (4.9) indicates that the random error associated with phase measurement is controlled by n and by the magnitude of $\gamma_{AB}^2(f)$.

The one-standard-deviation uncertainty, $\sigma\{X_{AL}\}$, in estimating the location of a leak with respect to sensor A, when sensors A and B bracket the leak and the mean propagation velocity, <V>, is measured between sensors B and C, is given by

$$\sigma\{X_{AL}\} = \frac{<V>}{4\pi}\left(\sigma\left\{\frac{d\phi_{AB}}{df}\right\}^2 + \left(\frac{<\frac{d\phi_{AB}}{df}>}{<\frac{d\phi_{BC}}{df}>}\right)\sigma\left\{\frac{d\phi_{BC}}{df}\right\}^2\right)^{1/2}. \tag{4.10}$$

Because the average rate of change of the phase with respect to frequency is directly related to physical distances, it can be shown that

$$\frac{<\frac{d\phi_{AB}}{df}>}{<\frac{d\phi_{BC}}{df}>} = \frac{(X_{AB}-2<X_{AL}>)}{X_{BC}}. \tag{4.11}$$

Assuming that $\sigma\{d\phi/df\} = \sigma\{d\phi_{AB}/df\} = \sigma\{d\phi_{BC}/df\}$, and using Eq. (4.11), Eq. (4.10) reduces to

$$\sigma\{X_{AL}\} = \frac{< V >}{4\pi} \sigma\left\{\frac{d\phi}{df}\right\} (1 + K^2)^{1/2}, \tag{4.12}$$

where

$$K^2 = \frac{(X_{AB} - 2 < X_{AL} >)^2}{X_{BC}^2}. \tag{4.13}$$

The uncertainty, $\sigma\{X_{AL}\}$, in the estimate of the location of the leak, X_{AL}, is affected by the three-sensor measurement geometry and the location of the leak. The term K accounts for this effect; clearly, the largest uncertainty occurs when K is largest. Eqs. (4.12) and (4.13) suggest that the minimum uncertainty in X_{AL} occurs when the leak is midway between A and B; in fact, when $X_{AL} = 0.5\ X_{AB}$, the uncertainty in X_{AL} is independent of the uncertainty, $\sigma\{d\phi_{BC}/df\}$, in the measurement of the propagation velocity. The maximum uncertainty in X_{AL} occurs when the leak is very near sensor A (or B), or when the separation distance, X_{BC}, used to estimate the propagation velocity is very small.

The estimates of uncertainty, $\sigma\{X_{AL}\}$, can be written in terms of the standard deviation of the phase, $\sigma\{\phi\}$, using the equation

$$\sigma\left\{\frac{d\phi}{df}\right\}^2 = \frac{N\sigma\{\phi\}^2}{N\Sigma f^2 - (\Sigma f)^2}, \tag{4.14}$$

where N is equal to the number of independent data points in the frequency band, Δf, used to estimate the rate of change of the phase. In general, there is some correlation between data points, and so the number of degrees of freedom is usually less than the number of data points used to derive $d\phi/df$. Estimates of $\sigma\{X_{AL}\}$ are made in the next section for different sensor geometries, levels of statistical significance, and frequency bands.

The most accurate estimates of leak location are made when (1) the number of independent data sets, n, used to compute coherence and phase, the number of degrees of freedom, N, and the frequency bandwidth used to estimate $d\phi/df$ are large, and (2) the leak is approximately at the mid-point between the two bracketing sensors.

4.3 Estimates of Measurement Uncertainty

A theoretical estimate of the standard deviation of the location estimate, $\sigma\{X_{AL}\}$, can be made with Eqs. (4.9), (4.12) and (4.14). A field estimate of $\sigma\{X_{AL}\}$ can be made, from repetitive measurements, with Eq. (4.10).

Figure 4.2 shows the uncertainty in phase determined from Eq. (4.9) as a function of the number of independent data segments, n, used to compute the coherence and for $\gamma^2_{AB}(f)$ = 0.2, 0.4, 0.6, and 0.8. When n = 15 (which is the number of independent data segments used in the leak location estimates in this paper), and $\gamma^2_{AB}(f) = 0.5$ (which is typical of the values of coherence for many of the leak location estimates), $\sigma\{\phi_{AB}(f)\} = 10.5°$.

Figures 4.3 through 4.5 show the uncertainty in the location estimate, $\sigma\{X_{AL}\}$, when the distances between sensors A and B and sensors B and C are nominally 38.1 m (125 ft) and 7.6 m (25 ft), respectively, and the distance between the leak and sensor A is 3.8 m (12.5 ft), 9.7 m (31.75 ft), and 19.0 m (62.5 ft). The curves are derived in terms of the number, n, of independent data segments used to estimate the coherence and $\gamma^2_{AB}(f)$. The estimates assume that $d\phi/df$ is computed from N = 26 points over the frequency band 2119 to 2373 Hz; the 254-Hz band represents the larger bands for which the location estimates were made. In many instances a frequency band closer to 100 Hz was used. The conditions used to generate Figure 4.6 are identical to those used to generate Figure 4.4, except that N = 5 points.

An estimate of the leak location and sensor separation is best made when the value of $\gamma^2(f)$ is significantly above the noise. Table 4.1 shows the one standard deviation in phase, sensor separation, and leak location as a function of n for the three geometries described above for values of $\gamma^2_{AB}(f)$ at the 95% and 99% levels of statistical significance. As n increases, the value of $\gamma^2_{AB}(f)$ required to maintain the same level of statistical significance decreases. Obviously, more accurate estimates of the location of the leak can be made if the values of $\gamma^2_{AB}(f)$ or n are greater than the values in Table 4.1. The results in Figures 4.3 through 4.5, as well as in Table 4.1, suggest that the largest uncertainty in leak location is less than 20 cm (7.88 in.).

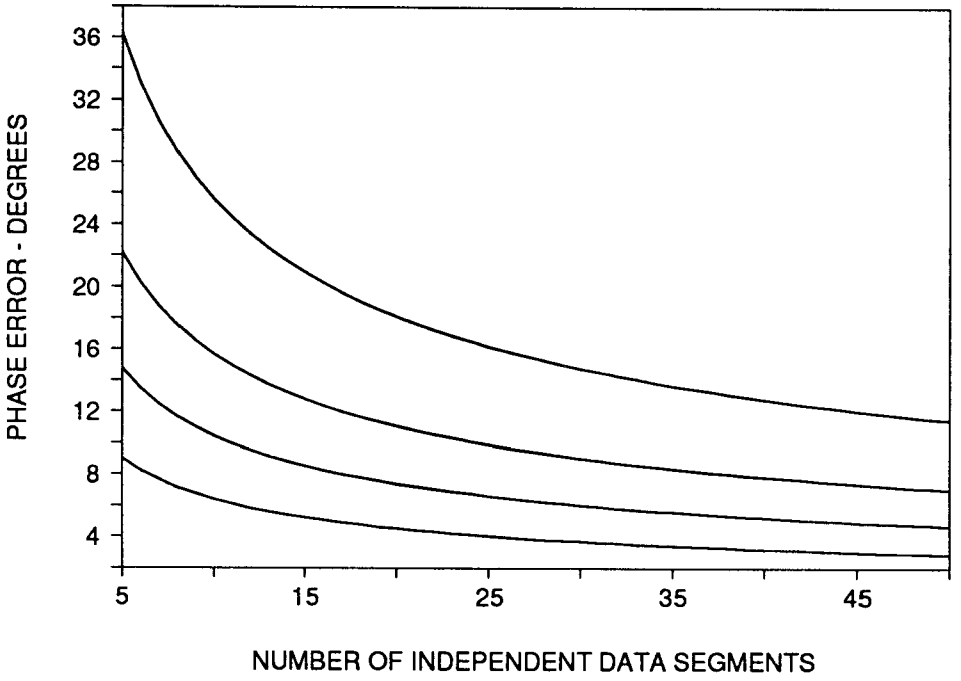

Figure 4.2. $\sigma\{\phi_{AB}(f)\}$ for sensor separation distance as a function of n between 5 and 50 and values of $\gamma^2_{AB}(f)$ equal to 0.8, 0.6, 0.4, and 0.2 estimated for any frequency with Eq. (4.9).

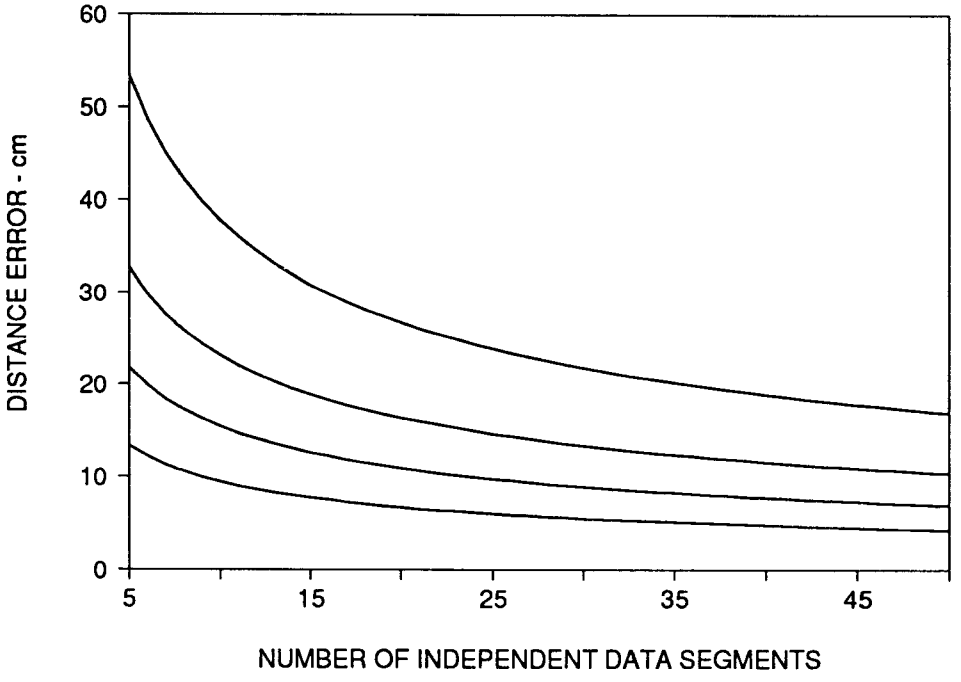

Figure 4.3. $\sigma\{X_{AB}\}$ for sensor separation distance between two sensors, A and B, as a function of n between 5 and 50 and values of $\gamma^2_{AB}(f)$ equal to 0.8, 0.6, 0.4, and 0.2 estimated with Eqs. (4.9), (4.12), and (4.14) for the following conditions: X_{AB} = 38.1 m (125 ft), X_{BC} = 7.6 m (25 ft), X_{AL} = 3.8 m (12.5 ft) (i.e., 10% of X_{AB}), Δf = 2373 - 2119 = 254 Hz, N = 26, and <V> = 1,000 m/s.

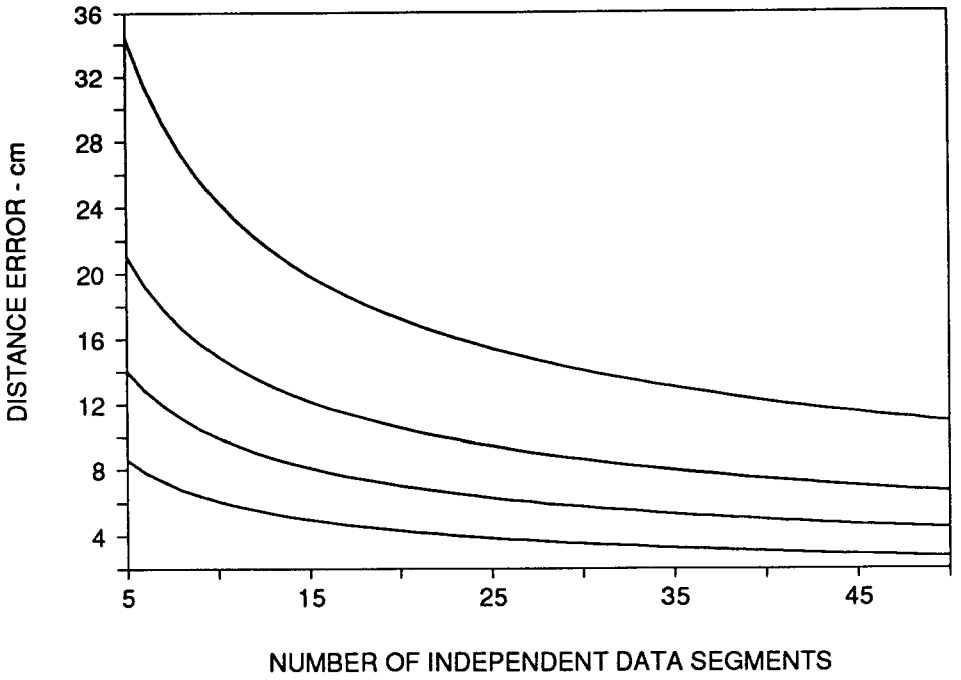

Figure 4.4. $\sigma\{X_{AB}\}$ for sensor separation distance between two sensors, A and B, as a function of n between 5 and 50 and values of $\gamma^2_{AB}(f)$ equal to 0.8, 0.6, 0.4, and 0.2 estimated with Eqs. (4.9), (4.12), and (4.14) for the following conditions: X_{AB} = 38.1 m (125 ft), X_{BC} = 7.6 m (25 ft), X_{AL} = 9.7 m (31.75 ft) (i.e., 25% of X_{AB}), Δf = 2373 - 2119 = 254 Hz, N = 26, and <V> = 1,000 m/s.

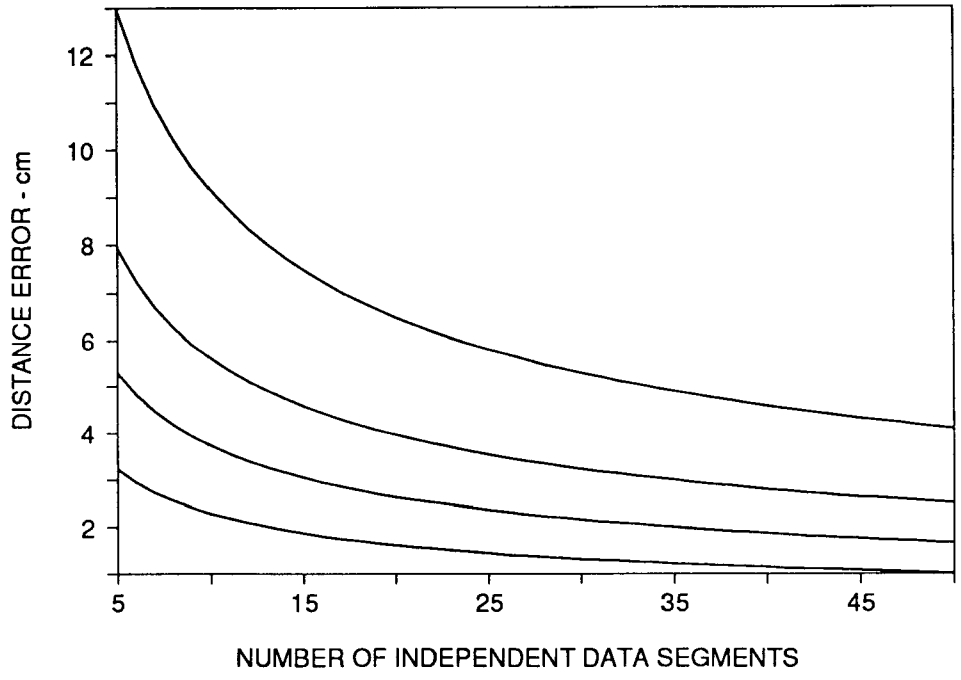

Figure 4.5. $\sigma\{X_{AB}\}$ for sensor separation distance between two sensors, A and B, as a function of n between 5 and 50 and values of $\gamma^2_{AB}(f)$ equal to 0.8, 0.6, 0.4, and 0.2 estimated with Eqs. (4.9), (4.12), and (4.14) for the following conditions: X_{AB} = 38.1 m (125 ft), X_{BC} = 7.6 m (25 ft), X_{AL} = 19.0 m (62.5 ft) (i.e., 50% of X_{AB}), Δf = 2373 - 2119 = 254 Hz, N = 26, and <V> = 1,000 m/s.

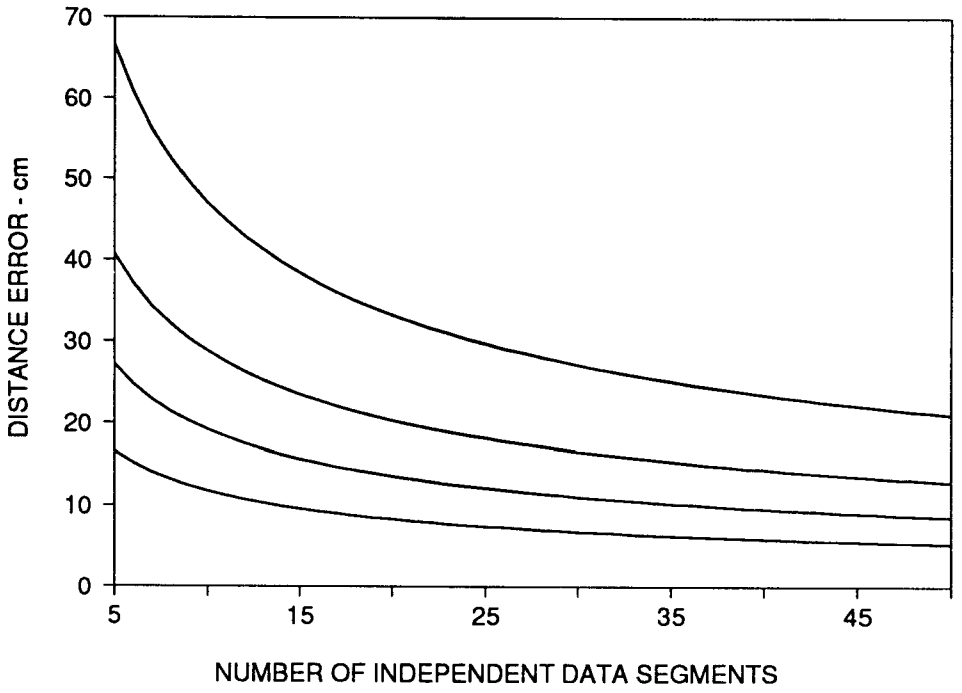

Figure 4.6. $\sigma\{X_{AB}\}$ for sensor separation distance between two sensors, A and B, as a function of n between 5 and 50 and values of $\gamma^2_{AB}(f)$ equal to 0.8, 0.6, 0.4, and 0.2 estimated with Eqs. (4.9), (4.12), and (4.14) for the following conditions: X_{AB} = 38.1 m (125 ft), X_{BC} = 7.6 m (25 ft), X_{AL} = 9.7 m (31.75 ft) (i.e., 25% of X_{AB}), Δf = 2373 - 2119 = 254 Hz, N = 5, and <V> = 1,000 m/s.

4.4 Accuracy

The accuracy of the acoustic measurement system for locating a leak along the pipeline is defined as the mean difference between the actual and estimated location of the leak. The accuracy is affected by any biases that may result from the phase measurement estimates, by the uncertainty in the estimate of the average propagation speed (as affected by an error in the location of the sensors with respect to each other), and by differences in the wave speed along different propagation paths from the leak to the sensors.

A bias in the phase measurements can occur for a variety of reasons: biases in the power spectral and cross spectral estimates used to compute phase, ambient noise that is highly directional, and other signals that are correlated with the input signal. These may include errors due to multiple modes of propagation that occur in the liquid product and the pipe wall and errors due to reflections of the signal within the pipe due to boundaries, joints, couplings, elbows, etc. Accurate theoretical estimates of bias errors are difficult to make and require information about the signal and noise field; as a consequence, none will be attempted here. It is anticipated, however, that the bias errors in the phase measurements will be small compared to the other two sources of error mentioned above.

Table 4.1. Estimates of the Total Uncertainty in Measuring the Separation between Sensors and the Location of a Leak as a Function of the Number of Incoherent Averages and $\gamma^2_{AB}(f)$ Computed for L = 95 and 99%

$\gamma^2_{AB}(f)$	Number of Averages	SNR	$\sigma\{\Phi_{AB}\}$ (o)	$\sigma\{X_{AB}\}^{*}$ (cm)	$\sigma\{X_{AL}\}^{**}$ (cm)	$\sigma\{X_{AL}\}^{***}$ (cm)	$\sigma\{X_{AL}\}^{****}$ (cm)
L = 95%							
0.78	5	3.5	9.7	35.5	14.3	9.2	3.5
0.49	10	0.9	13.2	48.0	19.4	12.5	4.7
0.35	15	0.5	14.3	52.2	21.1	13.6	5.1
0.27	20	0.4	14.9	54.3	21.9	14.1	5.3
0.22	25	0.3	15.2	55.5	22.4	14.4	5.4
0.12	50	0.1	15.9	57.9	23.4	15.1	5.7
L = 99%							
0.90	5	9.0	6.0	22.0	8.9	5.7	2.2
0.64	10	1.8	9.6	35.0	14.1	9.1	3.4
0.48	15	0.9	10.8	39.5	16.0	10.3	3.9
0.38	20	0.6	11.5	41.8	16.9	10.9	4.1
0.32	25	0.5	11.8	43.2	17.5	11.2	4.2
0.17	50	0.2	12.6	45.9	18.6	12.0	4.5

*Sensor separation error estimated between 2119 and 2373 Hz for V = 1,000 m/s and N = 26 assuming that the velocity is measured and the nominal sensor separations are X_{AB} = 38.1 m (125 ft) and X_{BC} = 7.6 m (25 ft), and X_{AL} = 9.7 m (31.75 ft).

**Leak location error estimated between 2119 and 2373 Hz for V = 1,000 m/s and N = 26 assuming that the velocity is measured and the nominal sensor separations are X_{AB} = 38.1 m (125 ft) and X_{BC} = 7.6 m (25 ft), and X_{AL} = 3.8 m (12.5 ft).

***Sensor separation error estimated between 2119 and 2373 Hz for V = 1,000 m/s and N = 26 assuming that the velocity is measured and the nominal sensor separations are X_{AB} = 38.1 m (125 ft) and X_{BC} = 7.6 m (25 ft), and X_{AL} = 9.7 m (31.75 ft).

****Leak location error estimated between 2119 and 2373 Hz for V = 1,000 m/s and N = 26 assuming that the velocity is measured and the nominal sensor separations are X_{AB} = 38.1 m (125 ft) and X_{BC} = 7.6 m (25 ft), and X_{AL} = 19.0 m (62.5 ft).

Ultimately, the accuracy of a leak location estimate depends on the speed of sound used to covert the time-of-arrival or phase measurements to distance. Any errors in the estimate of the wave propagation speed will translate directly into distance errors. Sound speed estimates should be measured experimentally to minimize these errors.

4.5 Performance of the Leak Location System

A leak *detection* system requires a high probability of detection (P_D) to be effective. The EPA regulation requires that a detection system have a P_D of at least 95%. On the other hand, a leak *location* system does not require a high P_D, but does require a low probability of false alarm (P_{FA}), 5% or less, to be effective. There is no recommended P_{FA} or P_D for a location system. However, a P_D of 50% or less should be sufficient because it is presumed that the leak location system is being used only *after* the existence of a leak has been confirmed.

The P_{FA} and P_D can be estimated directly from the SNR for normally distributed noise. These estimates can be made with the standard curves shown in Figure 4.7; these curves were reproduced directly from Urick [6] and can be found in many textbooks.

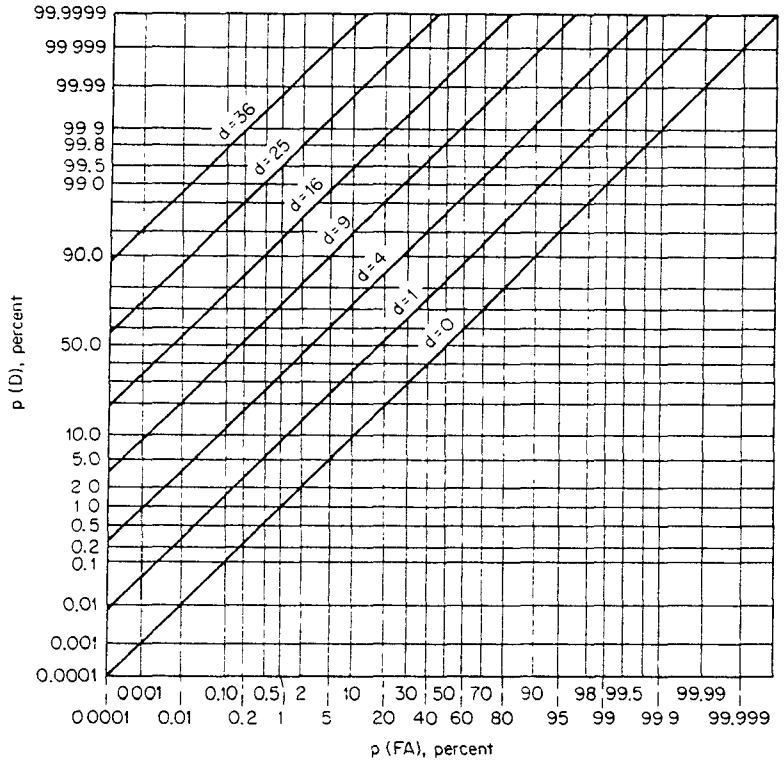

Figure 4.7. Estimates of P_D and P_{FA} as a function of SNR = d developed for normally distributed noise. (Urick [6])

Table 4.2 presents, as a function of SNR, estimates of the P_{FA} for a P_D of 50% and P_D for a P_{FA} of 5%. For most detection applications, an SNR over 9 will more than suffice. The P_{FA} and P_D can be further improved by averaging the results of multiple tests.

Table 4.2. Estimates of P_{FA} and a P_D of 50% as a Function of SNR

SNR	P_{FA} for $P_D = 50\%$ (%)	P_D for $P_{FA} = 5\%$ (%)
0	50	5
1	16	26
2	9	40
4	2.5	62
9	0.15	90
16	0.008	98
25	< 0.0001	99.93

The SNR can be computed from the coherence estimates made over the signal band of interest for any two sensors bracketing a leak in the pipeline [7]. The relationship between $\gamma^2(f)$ and the SNR is given by

$$SNR = \frac{\gamma^2(f)}{1-\gamma^2(f)}. \tag{4.15}$$

Eq. (4.8) can be used to estimate the probability of a false alarm as a function of SNR and the number of independent data segments used to compute the coherence. Thus, with Figure 4.7 (or Table 4.2) and Eqs. (4.8), and (4.15), (1) an estimate of the P_{FA} and P_D can be made for a leak location test based on the value of n used in the analysis and the value of $\gamma^2(f)$ measured, or (2) the minimum specifications of n and $\gamma^2(f)$ required to achieve a given P_{FA} and P_D can be estimated. The latter can be done by

- selecting the desired P_{FA} and P_D, and computing SNR from Figure 4.7,
- solving Eq. (4.15) for $\gamma^2(f)$ and computing $\gamma^2(f)$ for the SNR required to achieve the desired P_{FA} and P_D, and
- computing n from Eq. (4.8) for $\gamma^2(f)$ and P_{FA}.

The following example provides an estimate of the minimum number of independent data segments, n, and the minimum coherence, $\gamma^2(f)$, required to achieve a given performance. If a P_{FA} of 5% and a P_D of 50% are desired, the SNR estimated from Figure 4.7 must be approximately 3 (6 dB). The value of $\gamma^2(f)$ estimated from Eq. (4.15) is 0.75, and the value of n estimated from Eq. (4.8) is 5. If n is increased and the value of $\gamma^2(f)$ remains at 0.75, the P_{FA} will be less than 5% and the P_D will greater than 50%.

The P_D and P_{FA} can be estimated for a given measurement by

- computing the P_{FA} for a given n and the measured $\gamma^2(f)$ by means of Eq. (4.8),
- computing SNR for the measured $\gamma^2(f)$ by means of Eq. (4.15), and
- computing P_D for the given P_{FA} and SNR by means of Figure 4.7.

SECTION 5

EXPERIMENT DESIGN

The experiments were conducted on the pressurized 5-cm- (2-in.-) diameter steel pipeline at the UST Test Apparatus and were done in accordance with the quality assurance project plan [8]. A diagram of the pipeline at the UST Test Apparatus is shown in Figure 5.1. Access ports required for the attachment of transducers to the pipeline were located at intervals of approximately 8 m (25 ft); the coupling between the pipeline and an acoustic transducer is shown in Figure 5.2. Sensor positions shown in Figure 5.1 were used during all experiments. The transducers chosen for this work were CTI-30 resonant sensors. Though the CTI-30 is designed primarily for acoustic emissions applications, its sensitivity at low frequencies (1 to 5 kHz) is adequate for the detection of acoustic leak signals in pipelines. The acoustic signals were amplified by 80 dB, in two stages, by means of battery-operated Panametrics 5660-C preamplifiers and line-driven Krohn-Hite 3342 amplifying filters. A Western Graphtec TDA-3500 transient recorder was used to digitize the acoustic wave forms at a sampling rate of 10 kHz. Data were stored and analyzed with a COMPAQ-386 portable computer. A diagram of the data acquisition system is shown in Figure 5.3.

Figure 5.4 shows a diagram of the apparatus used to generate a leak in the pipeline. The flow rate of the leak was controlled by the static line pressure (0 to 172 kPa [0 to 25 psi]) and the diameter of the aperture through which the product was allowed to leak. Leak apertures between 0.3 and 0.8 mm (0.016 and 0.031 in.) were introduced into the pipeline via carburetor jets in order to avoid the difficulty of drilling small-diameter holes through the steel wall of the pipeline. The range of flow rates generated during the experiments was between 1.9 and 18.9 L/h (0.5 and 5.0 gal/h). The backfill materials used in the experiments were fine-grain sand and coarse gravel.

Three types of acoustic measurements (calibration, leak-on, and leak-off) were made for each combination of line pressure, hole diameter, and backfill material. The calibration signal was produced by breaking a pencil lead on the pipe surface near the location of the simulated leak. The relative arrival times of this impulsive signal at the three transducer locations were used to verify that the sensors and data acquisition system were operating properly. After the initiation of the leak, approximately eight leak-on measurements, each 1.7 s in duration, were recorded at 1-min intervals. The eight leak-on measurements were bracketed by a pair of recordings obtained under leak-off conditions.

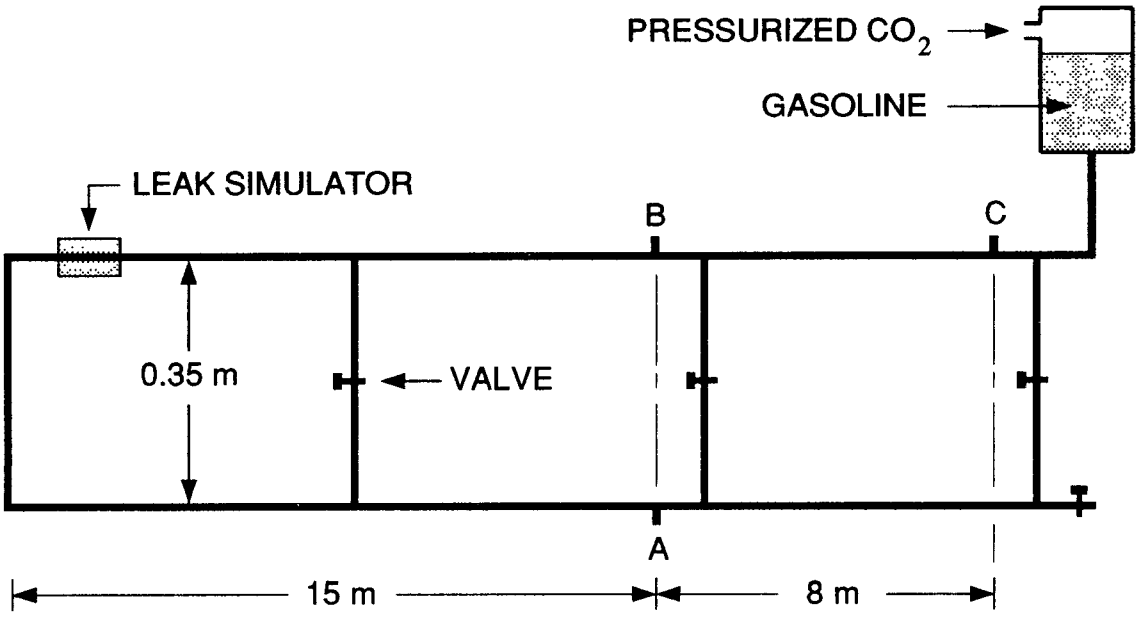

Figure 5.1. Diagram of the pressurized petroleum pipeline at the UST Test Apparatus. Pipe material is 5-cm-(2-in.-) diameter steel; product is gasoline. Pressurized CO_2 is used to generate 0- to 172-kPa (0- to 25-psi) static line pressure. Valves in connecting branches were closed during all experiments.

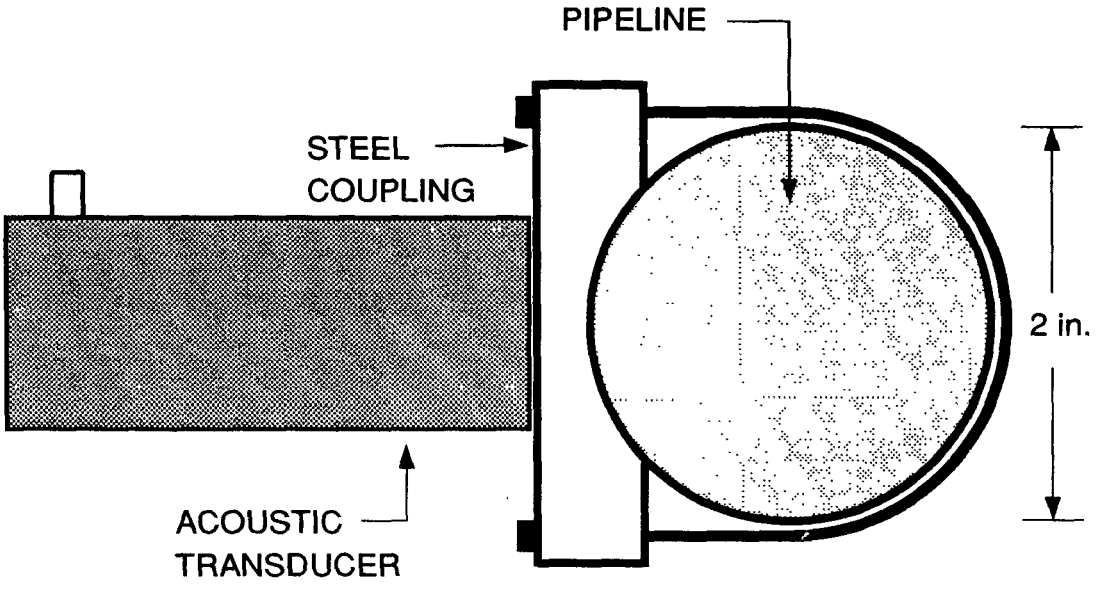

Figure 5.2. Diagram of the coupling between the acoustic transducer (CTI-30) and the steel pipeline.

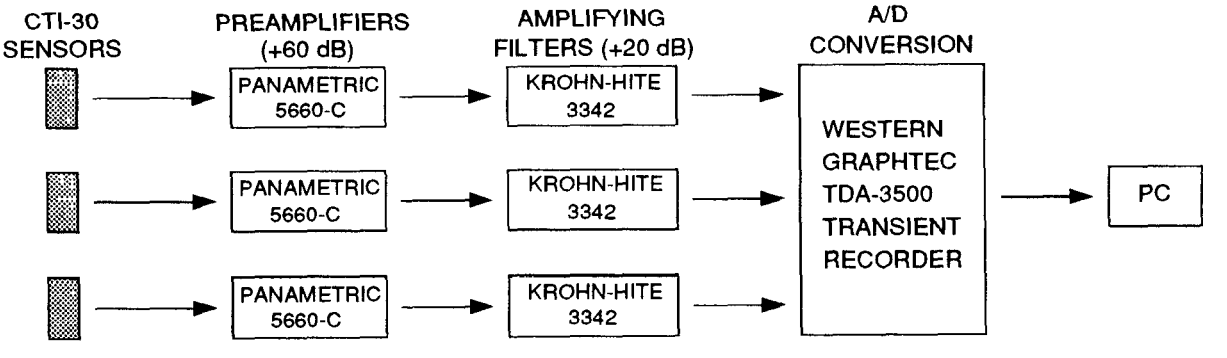

Figure 5.3. Diagram of the data acquisition system used in the experiments.

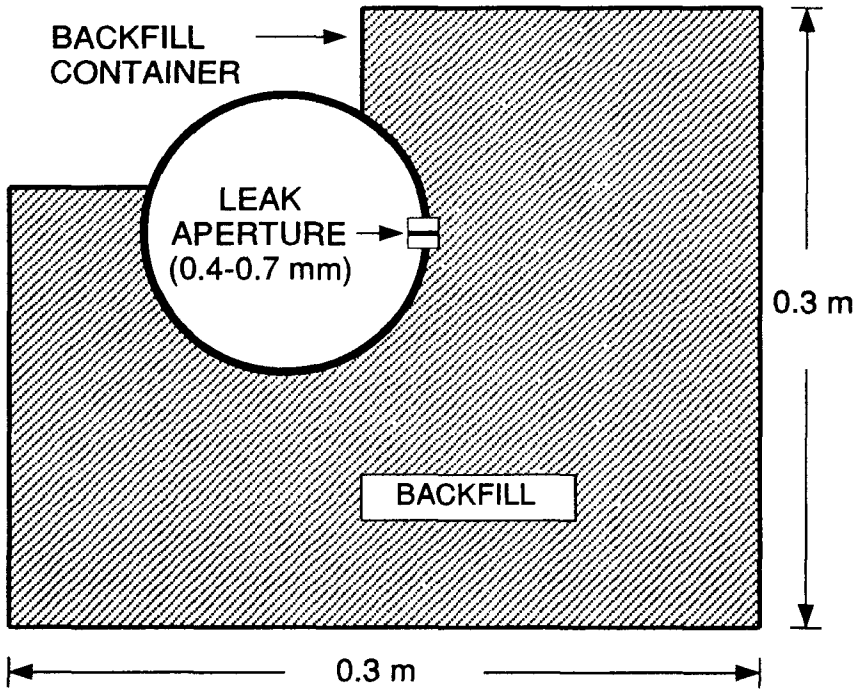

Figure 5.4. Apparatus used to generate simulated pipeline leak. Backfill materials are fine-grain sand and coarse gravel. Leak apertures between 0.3 and 0.8 mm (0.01 to 0.03 in.) were introduced into the pipeline via carburetor jets.

SECTION 6

DATA

The raw data consist of time series of acoustic leak signals and ambient noise sampled simultaneously by three sensors. The first step toward deriving and applying a leak location algorithm to the raw data is to view the data in three forms: (1) time series, (2) power spectral density, and (3) complex coherence. Viewed in the time domain, the leak-on and leak-off data (i.e., time series) provide convincing evidence that an acoustic leak signal exists and is detectable over the dimensions of the pipeline. In addition, the time series reveal the continuous character of the leak signal, as compared to the impulsive signal generated by the pencil-lead calibration signal. However, the time series alone offer no clues as to the location of the leak or the types of processing required to perform a source location estimate. The distribution, with respect to frequency, of acoustic energy emitted by the leak and the way in which this energy is propagated from source to sensor is revealed by viewing the data in the frequency domain (i.e., power spectra and complex coherence).

Time series of acoustic leak signals generated by a 11.4-L/h (3-gal/h) gasoline leak into a sand backfill are shown in Figure 6.1; a time series recorded under no-leak conditions by one of the sensors is shown for reference. Aside from an anti-alias filter applied to the analog signals prior to digitization, the time series shown here represent unfiltered data. The distance between the simulated leak and sensors A and B is approximately 15 m (50 ft); sensor C is located approximately 23 m (75 ft) from the leak. The line pressure used in this experiment was 103 kPa (15 psi) and the hole diameter was 0.7 mm (0.03 in). Two important observations are made regarding the time series of Figure 6.1: (1) the leak is clearly detectable from the difference between the leak-on and leak-off measurements, and (2) the relative arrival time of the leak signal at the different sensor locations cannot be obtained through inspection of the time series. The continuous nature of the acoustic leak signal requires that some type of signal processing be applied to the leak signal time series in order that the relative arrival times, and hence the location of the leak, can be estimated.

Figure 6.2 shows time series of acoustic leak signals generated by a 1.9-L/h (0.5-gal/h) leak into a sand backfill along with a no-leak time series for reference. The line pressure used in this experiment was 34 kPa (5 psi) and the hole diameter was 0.3 mm (0.014 in.); the sensor geometry is the same for all experiments. At the reduced flow rate of 1.9 L/h (0.5 gal/h), the

acoustic leak signal cannot be clearly identified in the raw time series. In order to detect the presence of small leaks, the data collected in the time domain must be transformed into the frequency domain.

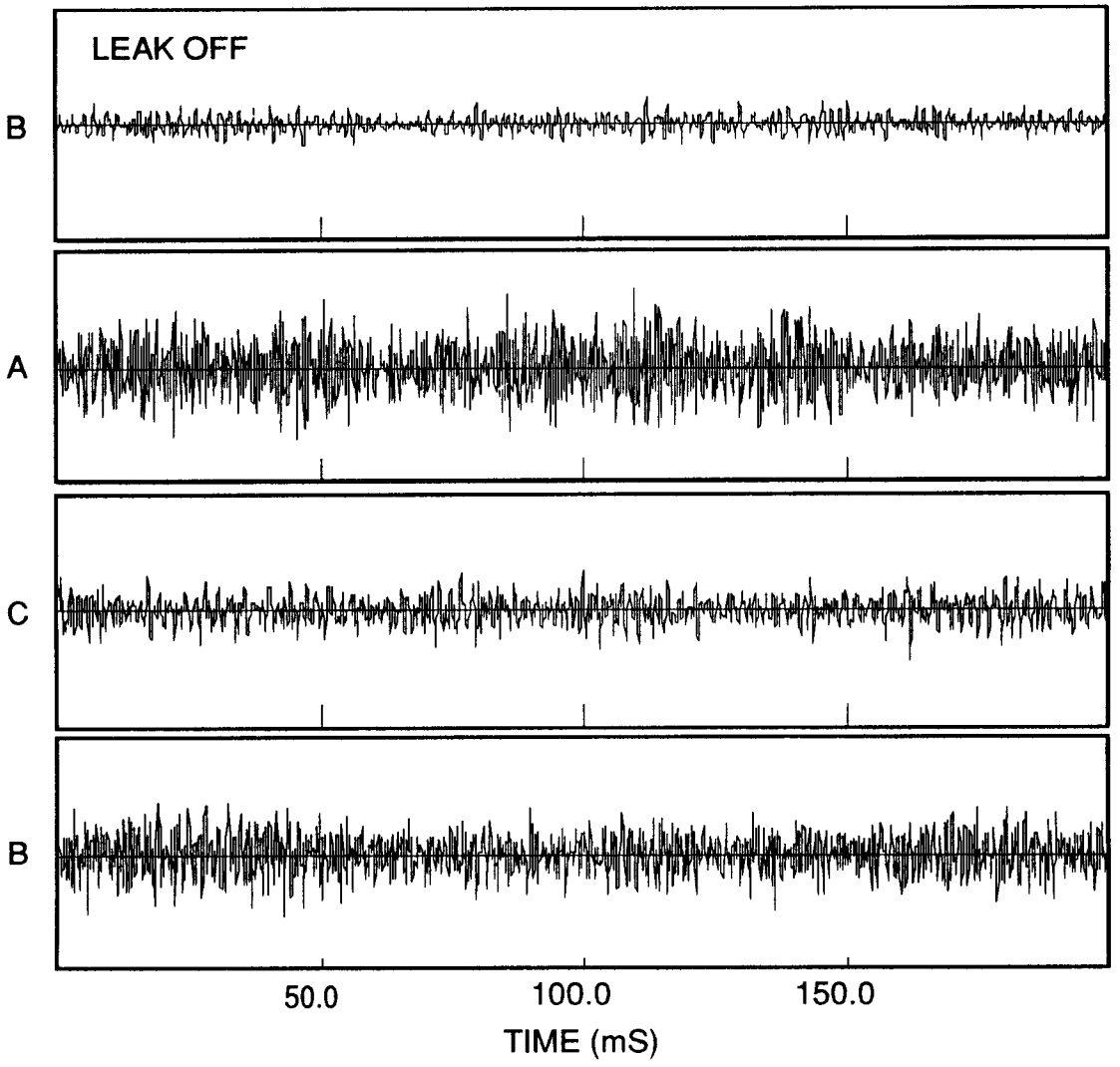

Figure 6.1. Time series of acoustic leak signals generated by a 11.4-L/h (3-gal/h) leak into a sand backfill. Line pressure is 103 kPa (15 psi) and hole diameter is 0.7 mm (0.03 in.). Sample rate is 10 kHz. A no-leak time series recorded by sensor B is shown for reference.

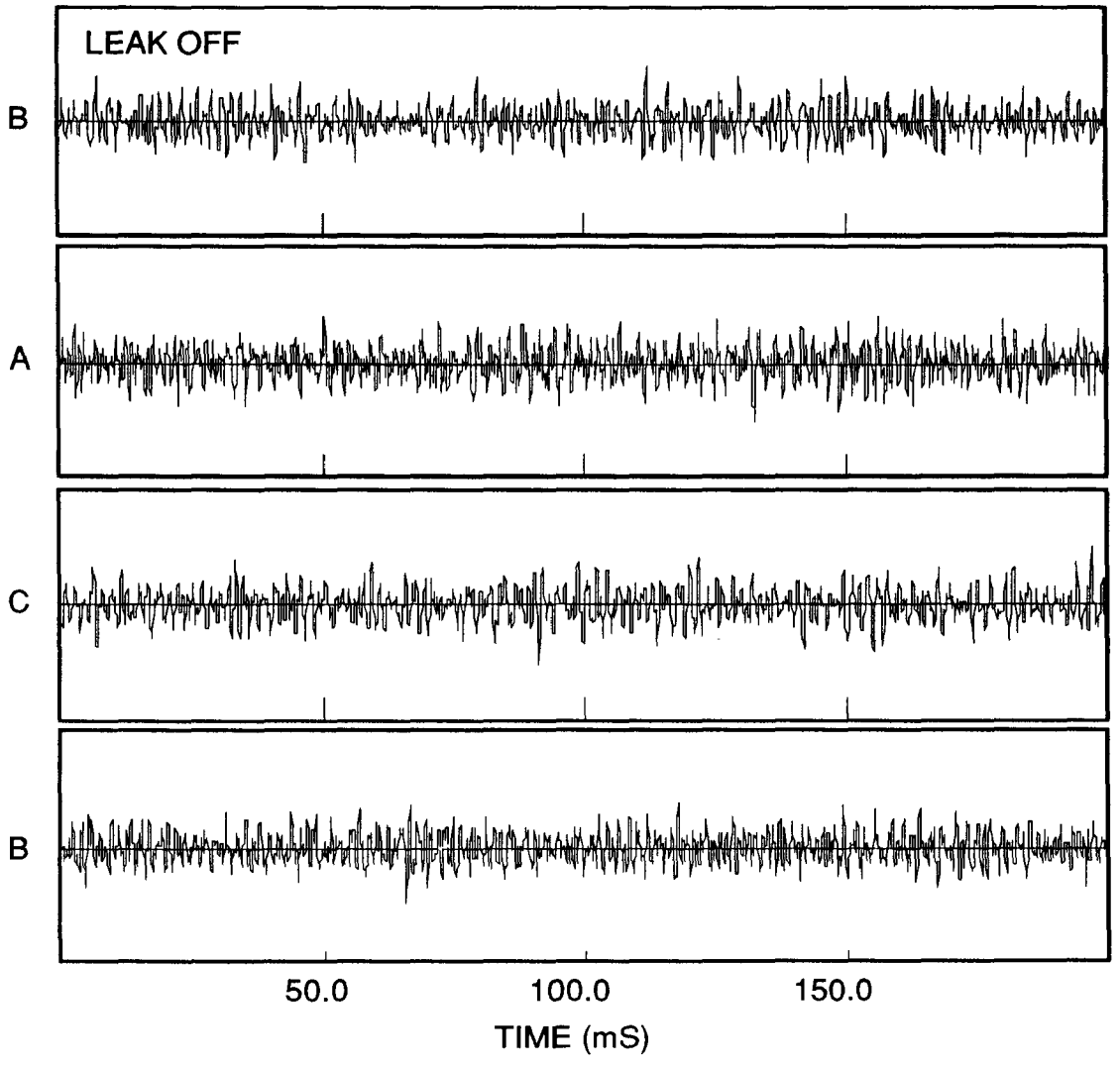

Figure 6.2. Time series of acoustic leak signals generated by a 1.9-L/h (0.5-gal/h) leak into a sand backfill. Line pressure is 34 kPa (5 psi) and hole diameter is 0.3 mm (0.01 in.). Sample rate is 10 kHz. A no-leak time series recorded by sensor B is shown for reference.

6.1 Signal Strength

The strength of the acoustic signal produced by a leak in a buried pipeline is primarily a function of flow rate, but is influenced somewhat by the surrounding backfill material. Estimates of the signal-to-noise ratio for pipeline leaks into a sand backfill at flow rates of 11.4, 5.7, 3.8 and 1.9 L/h (3.0, 1.5, 1.0 and 0.5 gal/h) are shown in Figures 6.3(a) through 6.3(d). The hole diameters and line pressures used to establish the flow rates were 0.7 mm at 103 kPa (15 psi) (i.e., 11.4 L/h [3.0 gal/h]); 0.5 mm at 103 kPa (15 psi) (i.e., 5.7 L/h) [1.5 gal/h]); 0.4 mm at 76 kPa (11 psi) (i.e., 3.8 L/h [1.0 gal/h]); and 0.4 mm at 34 kPa (5 psi)

(i.e., 1.9 L/h [0.5 gal/h]). The SNR at each flow rate was obtained by dividing the power spectral density computed with the leak present by a similar spectrum computed with no leak present. The power spectra for each of the three individual sensors, computed using 31 overlapping, 1024-point FFT segments, were averaged together prior to computing the SNR. The time series used were 1.7 s in duration and were sampled at a frequency of 10 kHz. The SNR spectra show that the energy associated with the acoustic leak signal is not equally distributed over the 1- to 5000-Hz sampling bandwidth, but is instead concentrated within a relatively narrow 1- to 4-kHz frequency band. The frequency domain representation of acoustic data offers a means by which the location algorithm can separate useful information concerning the leak from unwanted noise.

Figure 6.4 shows the SNR computed from time series recorded in the presence of an 11.4-L/h (3-gal/h) leak with coarse gravel as the backfill material. A comparison of Figures 6.4 and 6.3(a) indicates that the acoustic signal produced by the turbulent flow of product into a backfill of fine-grain sand represents a slight enhancement over that produced when the backfill consists of gravel. A similar relationship between the backfill material and the strength of the acoustic leak signal has been reported for studies of simulated leaks in the floor of aboveground storage tanks [9-11].

An estimate of the strength of the acoustic signal as a function of line pressure for a fixed-diameter hole is shown in Figure 6.5. The line pressures used in this experiment were 172 kPa (25.0 psi), 128 kPa (18.5 psi), 83 kPa (12.0 psi), and 41 kPa (6.0 psi); the hole diameter was 0.5 mm (0.020 in.). The average SNR computed over the 1- to 4-kHz frequency band is used as the measure of acoustic leak signal strength. As expected, the leak signal increases in strength as the line pressure is increased.

6.2 Coherence and Phase Measurements

Figure 6.6 shows the coherence amplitude and coherence phase as a function of frequency for acoustic leak signals received by sensors bracketing a 5.7-L/h (1.5-gal/h) leak. The sensor separation is 38 m (125 ft). The coherence plot represents an ensemble average of 15 overlapping, 1024-point segments, each individually detrended and weighted with a cosine bell prior to Fourier transforming. Statistically significant coherence (as indicated by the 95% confidence level) is observed primarily within the frequency bands 0.9 to 1.2 kHz and 2.0 to 4.0 kHz. It should be noted that within both of these frequency bands γ^2 is not statistically significant at all Fourier frequencies. Figure 6.7 shows the coherence amplitude, $\gamma^2(f)$, and coherence phase, $\phi(f)$, for acoustic leak signals received by sensors bracketing a

1.9-L/h (0.5-gal/h) leak. The sensor separation is 30 m (100 ft). As the flow rate is reduced (in this case by lowering the line pressure to 34 kPa [5 psi]), the frequency band within which signal similarity is maintained is narrowed considerably.

If the coherence amplitude is statistically significant for each Fourier component within a given frequency band, a simple phase-unwrapping procedure may be applied to the coherence phase. Figure 6.8 shows the unwrapped phase shift as a function of frequency between 3.8 and 4.0 kHz for sensors B and C of Figure 5.1; the flow rate is 11.4 L/h (3 gal/h).

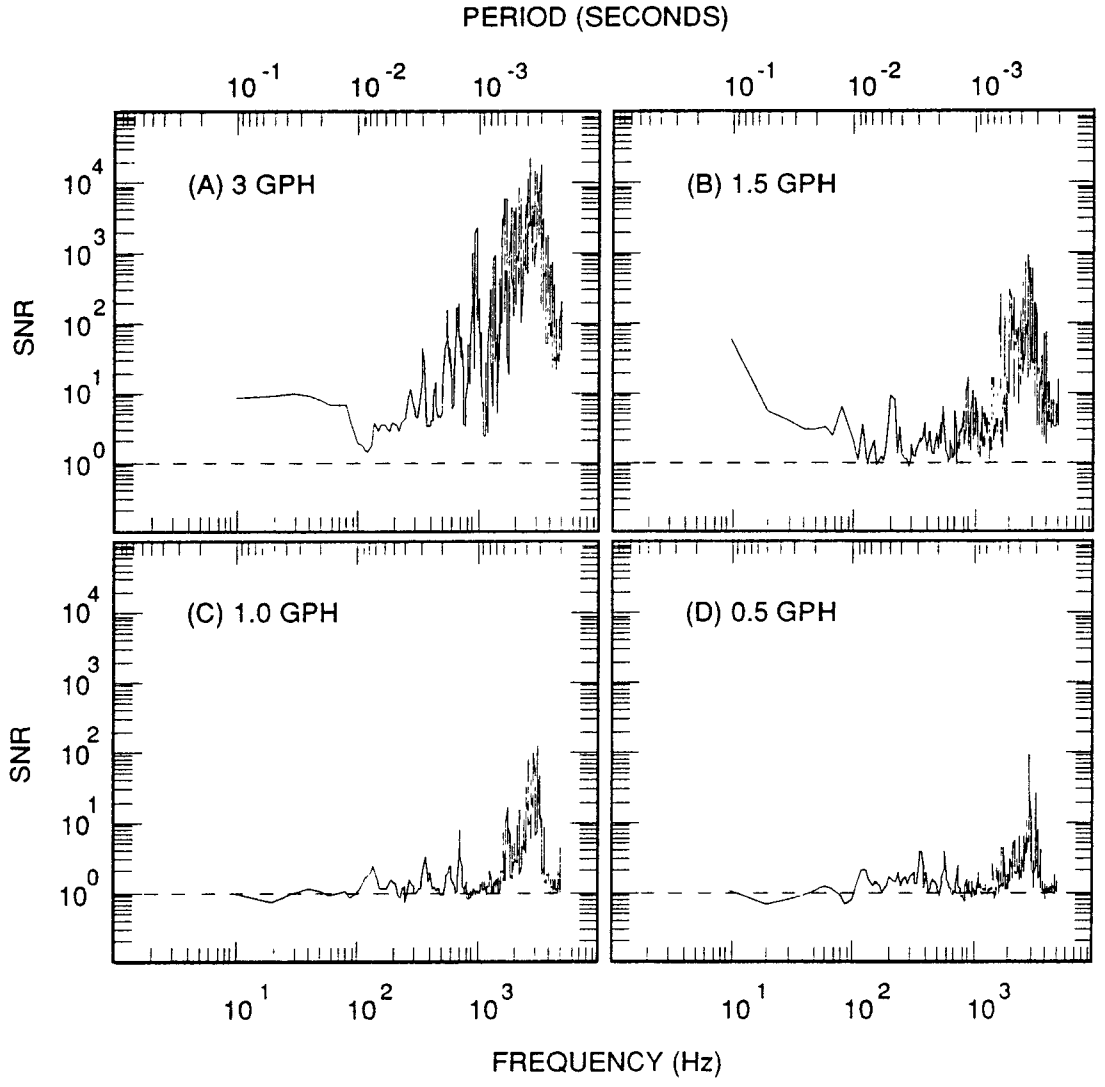

Figure 6.3. Signal-to-noise ratio (SNR) for pipeline leaks into a sand backfill at flow rates of 11.4 L/h (3.0 gal/h) (A), 5.7 L/h (1.5 gal/h) (B), 3.8 L/h (1.0 gal/h) (C), and 1.9 L/h (0.5 gal/h) (D). Dashed line indicates SNR=1. SNR estimates are computed by averaging the received power at each of the sensor locations shown in Figure 6.1.

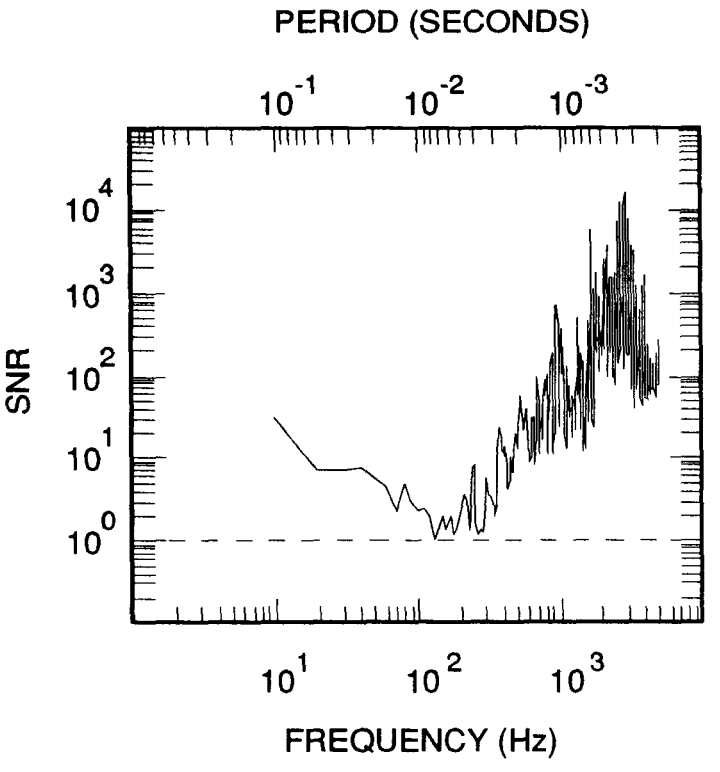

Figure 6.4. Signal-to-noise ratio (SNR) for pipeline leak into a gravel backfill. Flow rate is 11.4 L/h (3.0 gal/h).

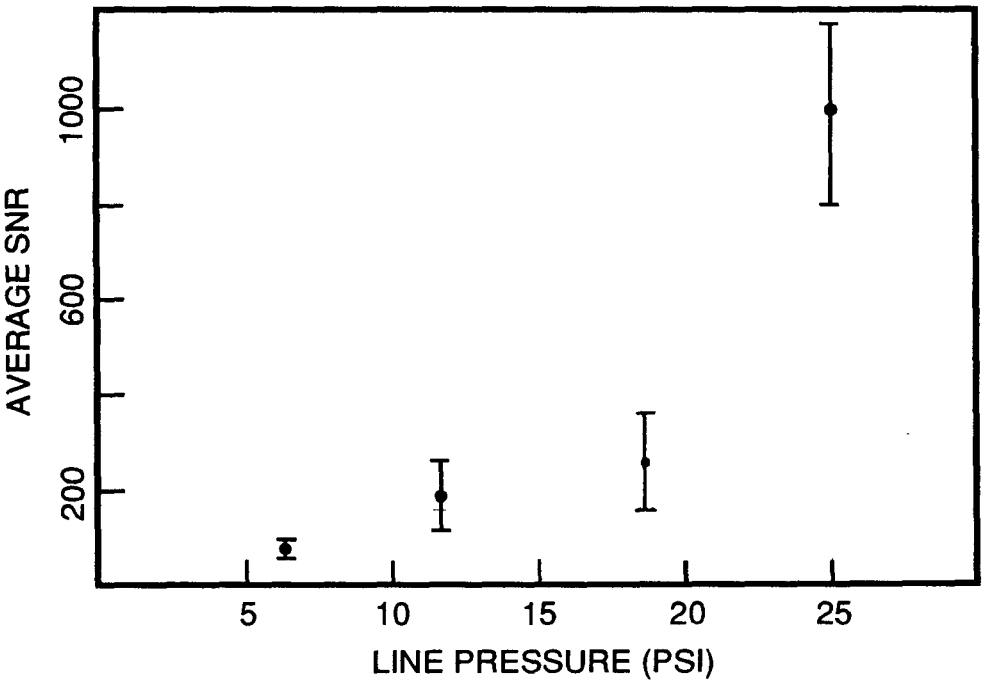

Figure 6.5. Strength of acoustic leak signal as a function of static line pressure for a fixed hole diameter (0.5 mm [0.02 in]). Error bars indicate the standard deviation of six measurements used to compute the SNR at each pressure level.

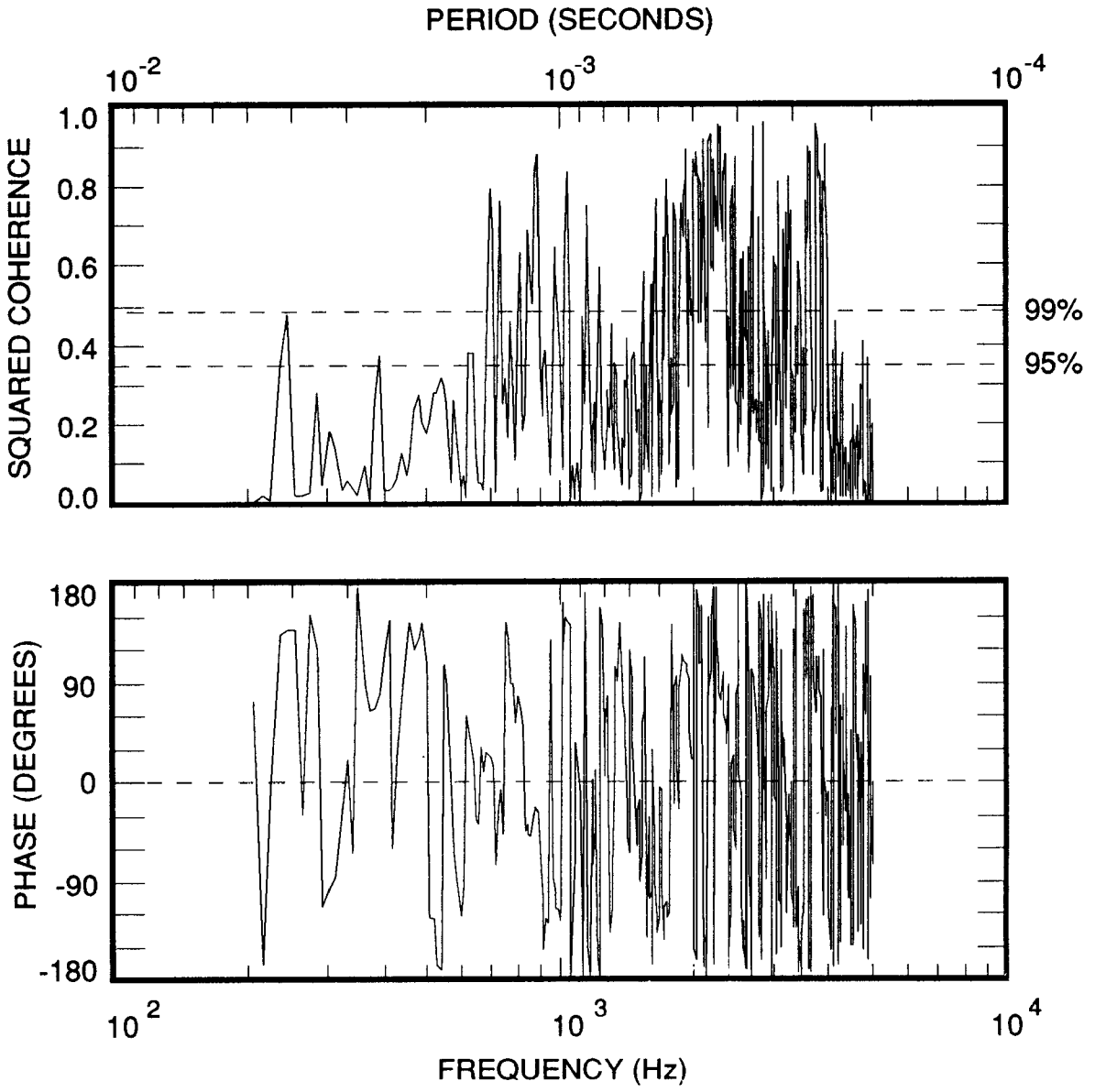

Figure 6.6. Coherence amplitude and coherence phase as a function of frequency for acoustic leak signals bracketing a 5.7-L/h (1.5-gal/h) leak. Sensor separation is 38.1 m (125 ft). The coherence function represents an ensemble average of 15 overlapping, 1024-point data segments. Dashed lines indicate 95% and 99% levels of statistical significance.

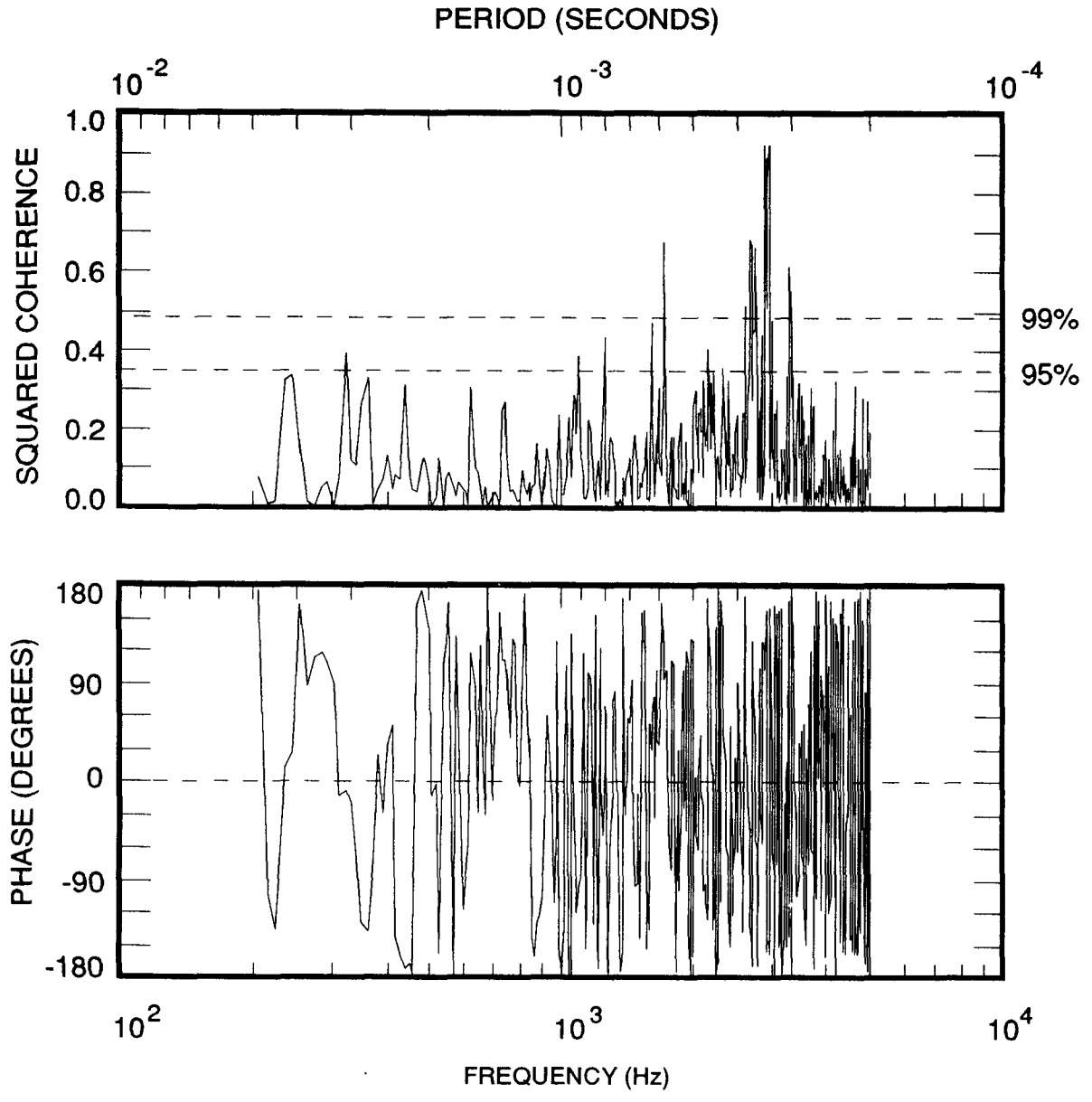

Figure 6.7. Coherence amplitude and coherence phase for acoustic leak signals bracketing a 1.9-L/h (0.5-gal/h) leak. Line pressure is 34 kPa (5 psi); sensor separation is 30 m (100 ft). Dashed lines indicate 95% and 99% levels of statistical significance.

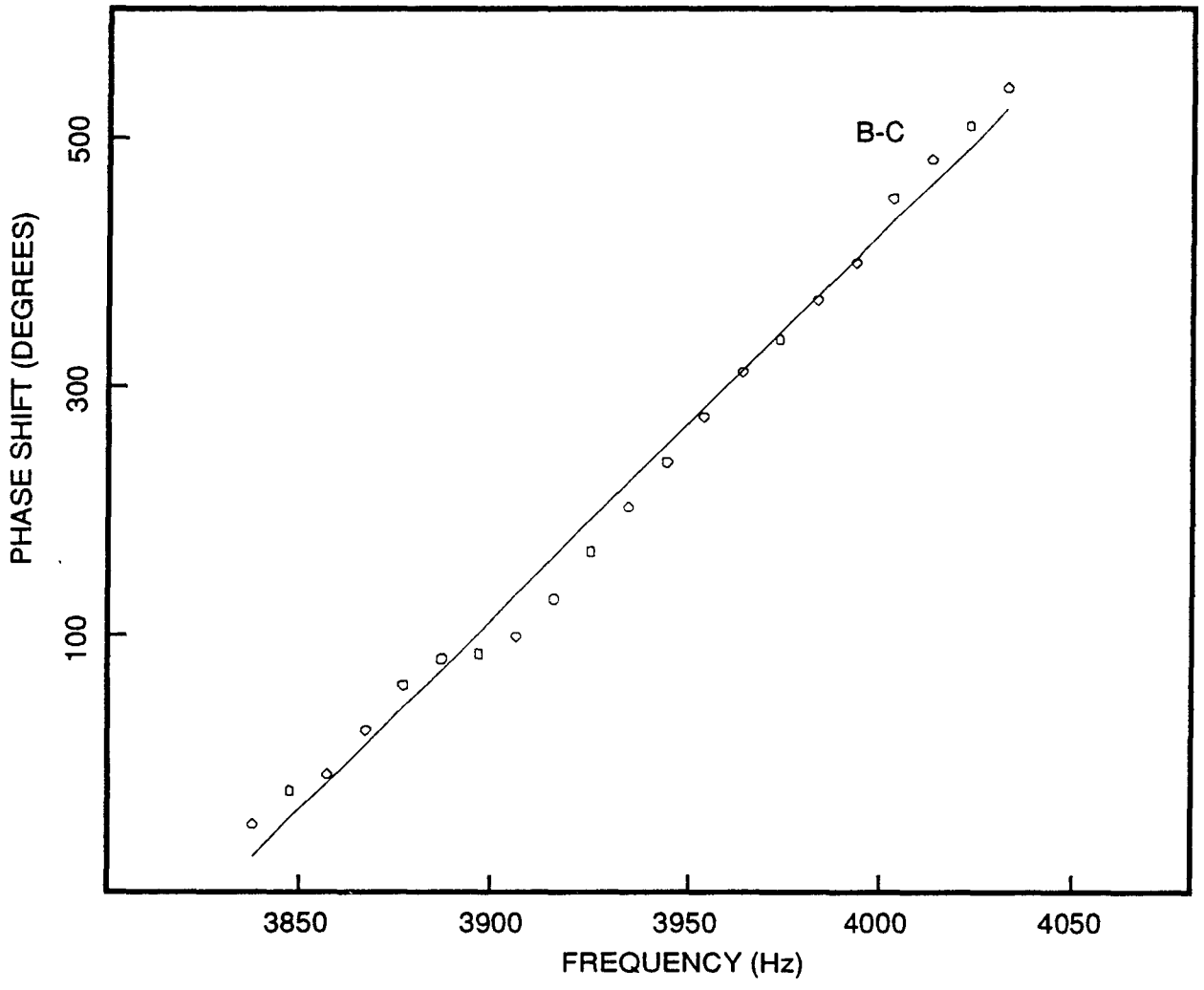

Figure 6.8. Unwrapped coherence phase, $\phi(f)$, between 3.8 and 4.0 kHz for sensor pair B-C of Figure 5.1. Least-squares regression line through actual data points is included. The flow rate is 11.4 L/h (3 gal/h).

SECTION 7

LOCATION RESULTS

The procedure used to estimate the leak location and wave speed for a given set of time series is as follows: (1) compute the coherence function between the three sensor pairs (i.e., A-B, A-C, and B-C), (2) identify frequency bands of at least 100-Hz width for which the coherence amplitude exceeds the 95% level of statistical significance, (3) unwrap the coherence phase within these frequency bands, (4) compute the linear regression lines through each of the three $\phi(f)$ curves, and (5) apply Eqs. (4.5) through (4.7) using the known sensor positions and the computed regression slopes.

Figure 7.1 shows the unwrapped phase differences between sensor pairs A-B, A-C, and B-C for the frequency band 2.0 to 2.5 kHz. The flow rate used in this experiment was 11.4 L/h (3 gal/h). Included in this plot are least-squares regression lines through the actual data points corresponding to each sensor pair. The criterion for the inclusion of a phase measurement in the estimation of leak location and wave speed is that the coherence amplitude exceed the 95% level of statistical significance for each of the three sensor pairs at a given Fourier frequency. Table 7.1 summarizes the results of leak location and wave speed estimates for flow rates of 11.4, 5.7, and 3.8 L/h (3.0, 1.5, and 1.0 gal/h). Leak location estimates are reported as a difference between the computed and actual location.

The regression slopes of Figure 7.1 can be used to calculate the time delays between signals received by the three sensor pairs. The measured $d\phi/df$ values of -0.47°/Hz (A-B), 2.07°/Hz (A-C), and 2.55°/Hz (B-C) correspond to time delays of -1.3 ms, 5.8 ms, and 7.1 ms, respectively.

An alternative method of extracting the time delays from the time series is to apply the technique of cross-correlation. Figure 7.2 shows the normalized cross-correlation coefficient, $\rho_{xy}(\tau)$, as a function of lag time (τ) between time series recorded by sensors B and C. The time series were bandpass-filtered in order to isolate the high SNR portion of the leak signal spectrum (1 to 4 kHz) prior to computing the correlation coefficient. Without the detailed knowledge of the distribution of leak signal energy provided by the coherence function, correlation analysis fails to give an accurate measurement of the time delay between leak signals received by sensors B and C. Figure 7.3 shows the correlation coefficient computed between B and C time series in which the data are bandpass-filtered from 2.0 to 2.5 kHz. Within the high-coherence interval

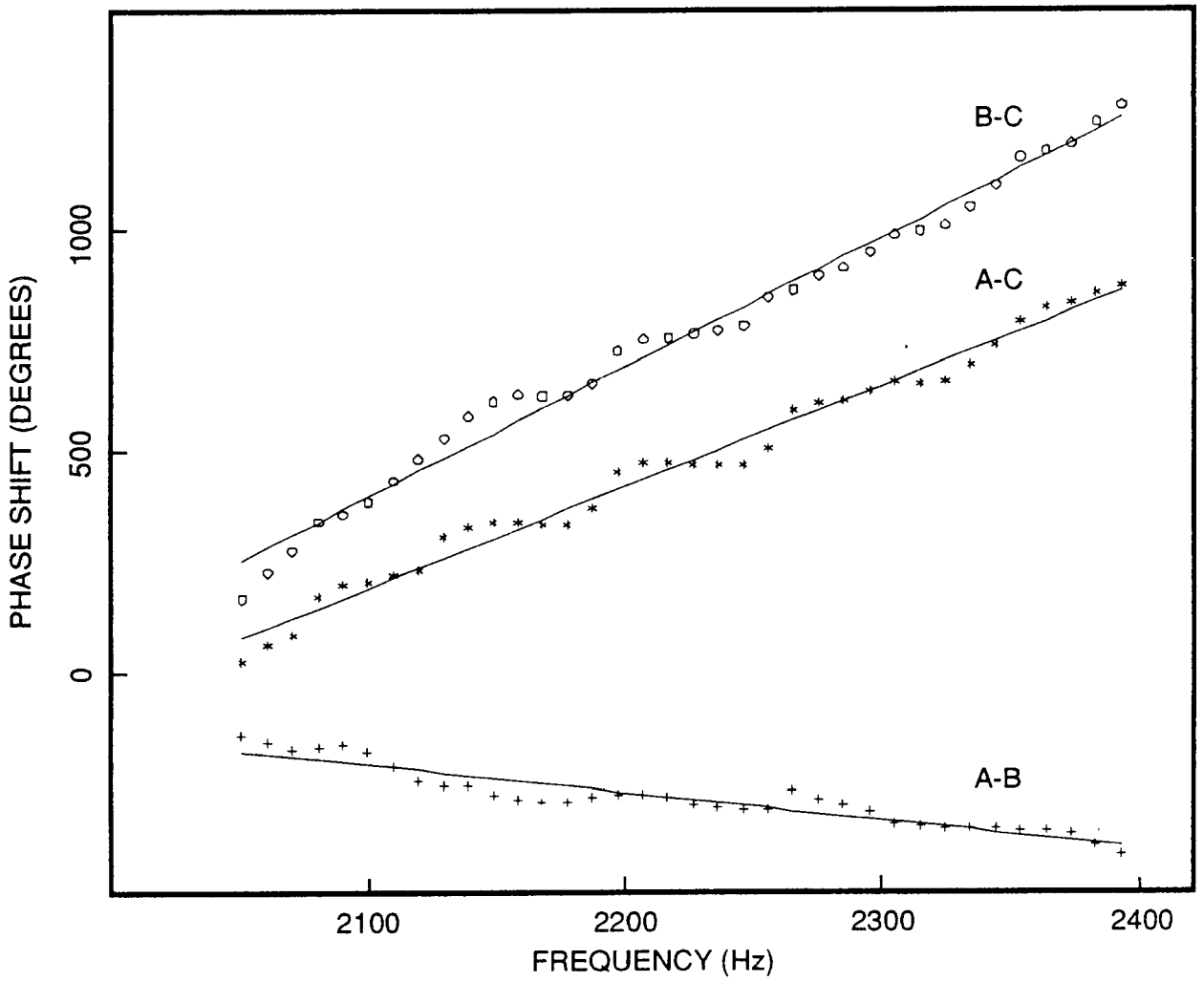

Figure 7.1. Unwrapped coherence phase between 2.0 and 2.5 kHz for sensor pairs A-B, A-C, and B-C of Figure 5.1. Least-squares regression lines through actual data points are included. The flow rate is 11.4 L/h (3 gal/h).

used to generate the phase curves of Figure 7.1, correlation analysis and coherence function analysis result in approximately equal estimates of the time delay. Although this result suggests that the two techniques for measuring time delays are equivalent, accurate correlation analysis requires *a priori* knowledge of the frequency bands within which the acoustic leak signal is strong and composed of linearly propagating waves. Coherence function analysis identifies frequency bands for which the SNR is high (through the coherence amplitude) and for which the phase behavior is appropriate for leak location (through the coherence phase).

Table 7.1. Leak Location and Propagation Speed Measurements

Flow Rate[1] (L/h)	D (mm)	P[2] (kPa)	Δf[3] (Hz)	Mean Error (AB)[4] (cm)	Std. Dev. (AB)[4] (cm)	Mean Error (AC)[5] (cm)	Std. Dev. (AC)[5] (cm)	V (m/s)	σV (m/s)	N^6_{LOC}
11.4	0.7	138	2100 - 2400	8.6	16.4	-2.4	23.7	1048	37	25
11.4	0.7	138	3800 - 4050	18.7	29.9	14.2	31.8	917	89	18
5.7	0.5	138	2100 - 2400	14.4	15.8	15.8	14.9	930	136	23
5.7	0.5	138	3800 - 4050	-5.8	19.8	-12.2	20.4	775	81	15
3.8	0.5	76	3800 - 4050	-2.5	47.9	-20.7	28.1	715	150	8

1) 11.4 L/h = 3.0 gal/h; 5.7 L/h = 1.5 gal/h; and 3.8 L/h = 1.0 gal/h
2) 128 kPa = 20 psi and 76 kPa = 11 psi
3) Location Algorithm Analysis Band
4) A-B used as bracketing sensors
5) A-C used as bracketing sensors
6) Number of independent location estimates

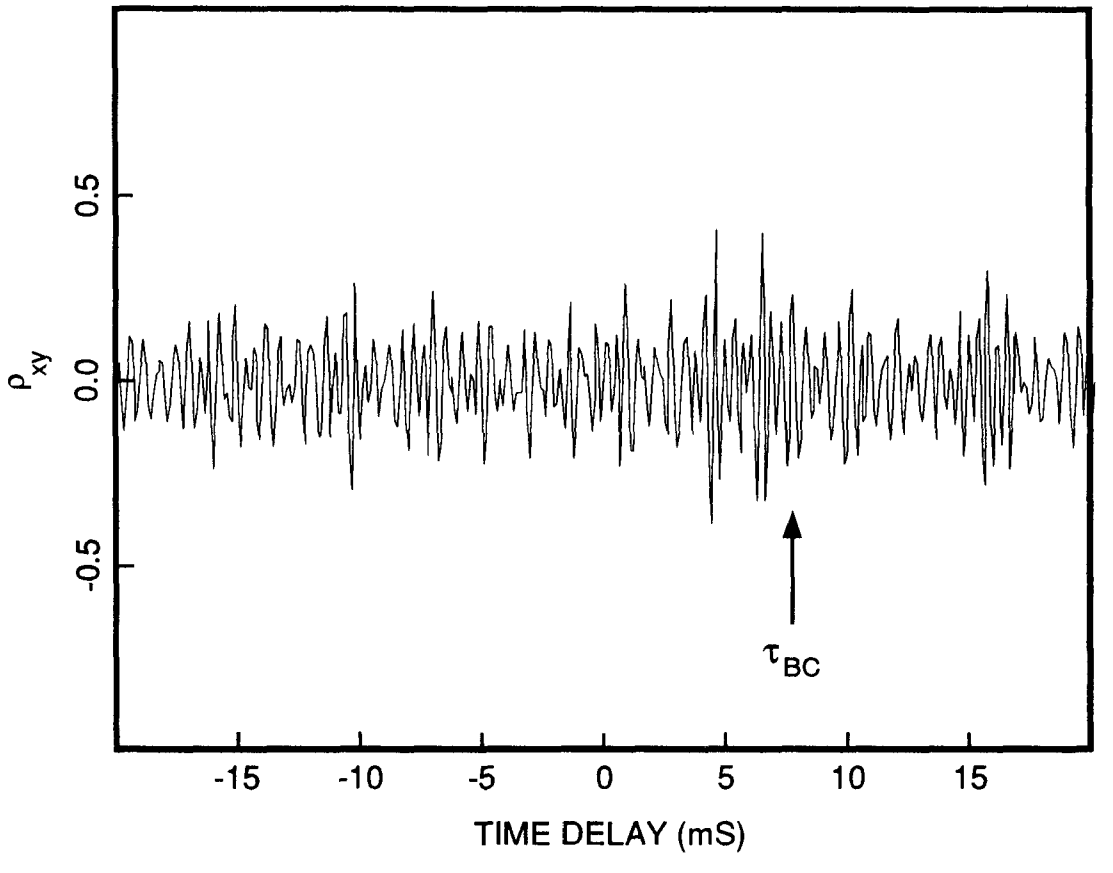

Figure 7.2. Normalized cross-correlation coefficient, $\rho_{xy}(\tau)$, as a function of time delay (τ) between time series recorded by sensors B and C. The time series were bandpass-filtered between 1.0 and 4.0 kHz prior to computing ρ_{xy}. The flow rate is 11.4 L/h (3 gal/h). τ_{BC} represents the predicted B-C time delay at V = 1000 m/s.

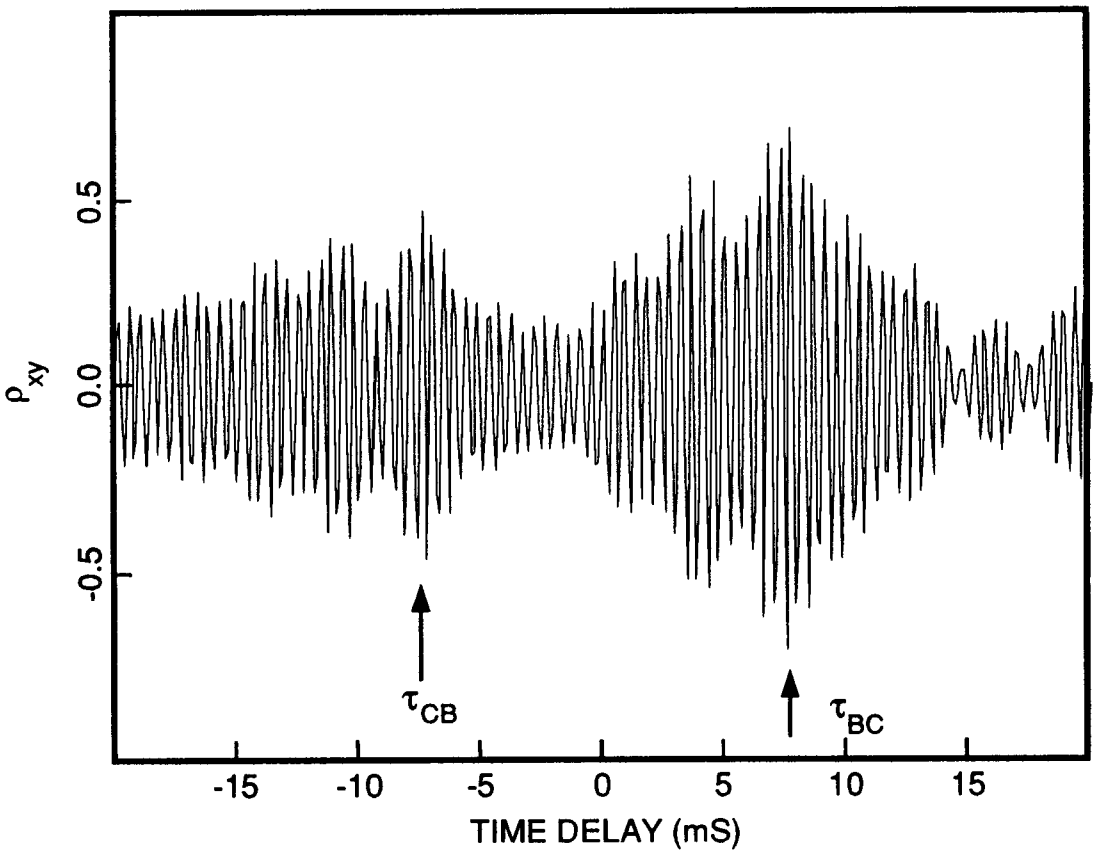

Figure 7.3. Normalized cross-correlation coefficient as a function of time delay between time series recorded by sensors B and C. The time series were bandpass-filtered between 2.0 and 2.5 kHz prior to computing ρ_{xy}. The flow rate is 11.4 L/h (3 gal/h). τ_{BC} and τ_{CB} represent predicted time delays for primary and reflected acoustic waves propagating at V = 1000 m/s.

SECTION 8

LEAK SIGNAL PROPAGATION

The analysis of acoustic data from pipelines is complicated by the presence of multi-path and multi-mode wave propagation. Multi-path signals are produced by reflections within the complex pipeline geometry or by signal leakage, across the connecting arms, from one main branch of the pipeline to the other (see Figure 5.1). Multi-mode wave propagation results from the excitation, by the leak flow field, of wave motion in different materials (e.g., gasoline and steel), or of waves in the same material that propagate at different speeds (e.g., longitudinal and transverse waves). While the analysis presented above suggests that the acoustic leak signal is dominated by a single propagation mode that traverses a single path from leak to sensor, experimental data and simple simulations show that the effects of multi-path and multi-mode propagation are detectable.

The reflective nature of the pipeline is illustrated by the cross-correlation plot shown in Figure 7.3. The primary ρ_{xy} peak, which occurs at the lag time $\tau \sim 7$ ms, corresponds to signals propagating in the direction from sensor B to sensor C at speed $c \sim 1000$ m/s. A secondary peak, which occurs at the lag time $\tau \sim -7$ ms, is consistent with reflection signals propagating at the same speed, but in the opposite direction.

Energy propagation along the pipeline results from the excitation of three types of wave motion by the leak flow field: (1) transverse waves propagating in the steel, (2) longitudinal waves propagating in the steel, and (3) longitudinal waves propagating within the product contained in the pipeline. The nominal propagation speeds for each type of wave motion are 6,000 m/s (longitudinal, steel), 3,000 m/s (transverse, steel), and 1,200 m/s (longitudinal, gasoline). The similarity between the measured wave speed (~ 1000 m/s) and the speed of acoustic waves in gasoline suggests that in the far field of the leak, the sensors respond primarily to longitudinal waves propagating through the product. These longitudinal waves are sensed indirectly through stresses induced in the steel in response to the fluctuating pressure field within the pipe. If other forms of wave motion are produced by the leak and are detectable, the phase measurements, and thus the location estimates, will be degraded. The detectability of longitudinal waves propagating in steel was investigated through a calibration test in which an impulsive signal was generated by the breaking of a pencil lead near the leak location. Figure 8.1 shows the time series of the calibration impulse received by sensors B and C. The measured time delay (1.2 ms) and sensor separation (7.5 m) yield a propagation speed of 6,250 m/s for the leading

edge of the impulse. This speed is consistent with the nominal value of 6,000 m/s for longitudinal waves propagated within the steel. While the calibration data do not indicate the degree to which the longitudinal wave mode in steel is excited by the leak flow field, it does show that such waves, if excited by the leak, will be detected by sensors mounted externally on the pipeline wall.

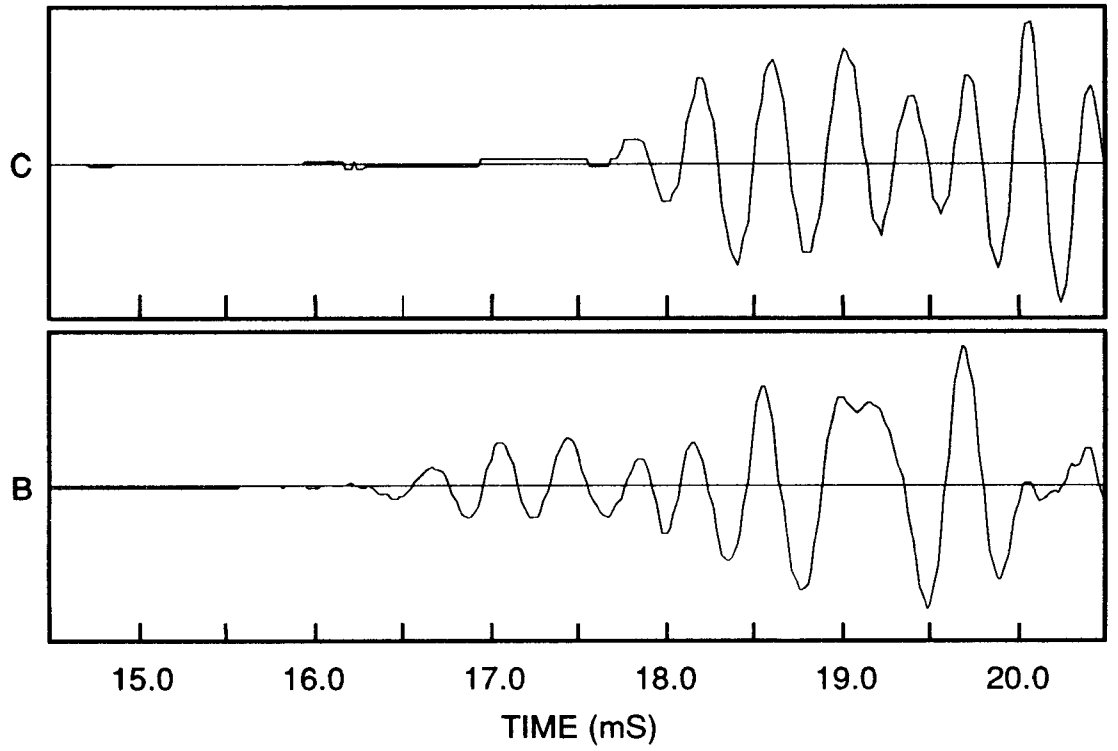

Figure 8.1. Time series of impulsive calibration signals recorded by sensors B and C of Figure 5.1. The estimated propagation speed (6250 m/s) is consistent with the nominal speed of sound in steel.

The excitation of transverse waves by the leak flow field, and their detectability, were investigated through a series of experiments in which CO_2, rather than gasoline, was used as the product. Figure 8.2 shows the unwrapped phase shift between sensors B and C measured in the presence of a 103-kPa (15-psi), CO_2 leak. The hole diameter was 7 mm (0.029 in.). Application of Eq. (4.7) to the phase plot yields a propagation speed of approximately 2,400 m/s. Two important observations should be noted regarding this experiment: (1) the measured wave speed is similar to the nominal value for transverse waves propagating freely in steel, and (2) the measured wave speed is much higher than the speed of acoustic waves propagated in CO_2 ($c \sim 270$ m/s). The SNR of the CO_2 leak was approximately 15 dB less than the SNR recorded in the presence of a gasoline leak at the same line pressure and hole diameter. Two conclusions may be drawn from these measurements: (1) freely propagating transverse waves are produced

by the leak and are detectable in the far field, and (2) the coupling between acoustic waves in the product and stresses induced in the surrounding pipeline is a function of the product contained within the pipeline. Liquid leaks appear to be sensed primarily through energetic, low-velocity acoustic waves, while gas leaks are sensed via less energetic, high-velocity transverse waves propagating in the steel.

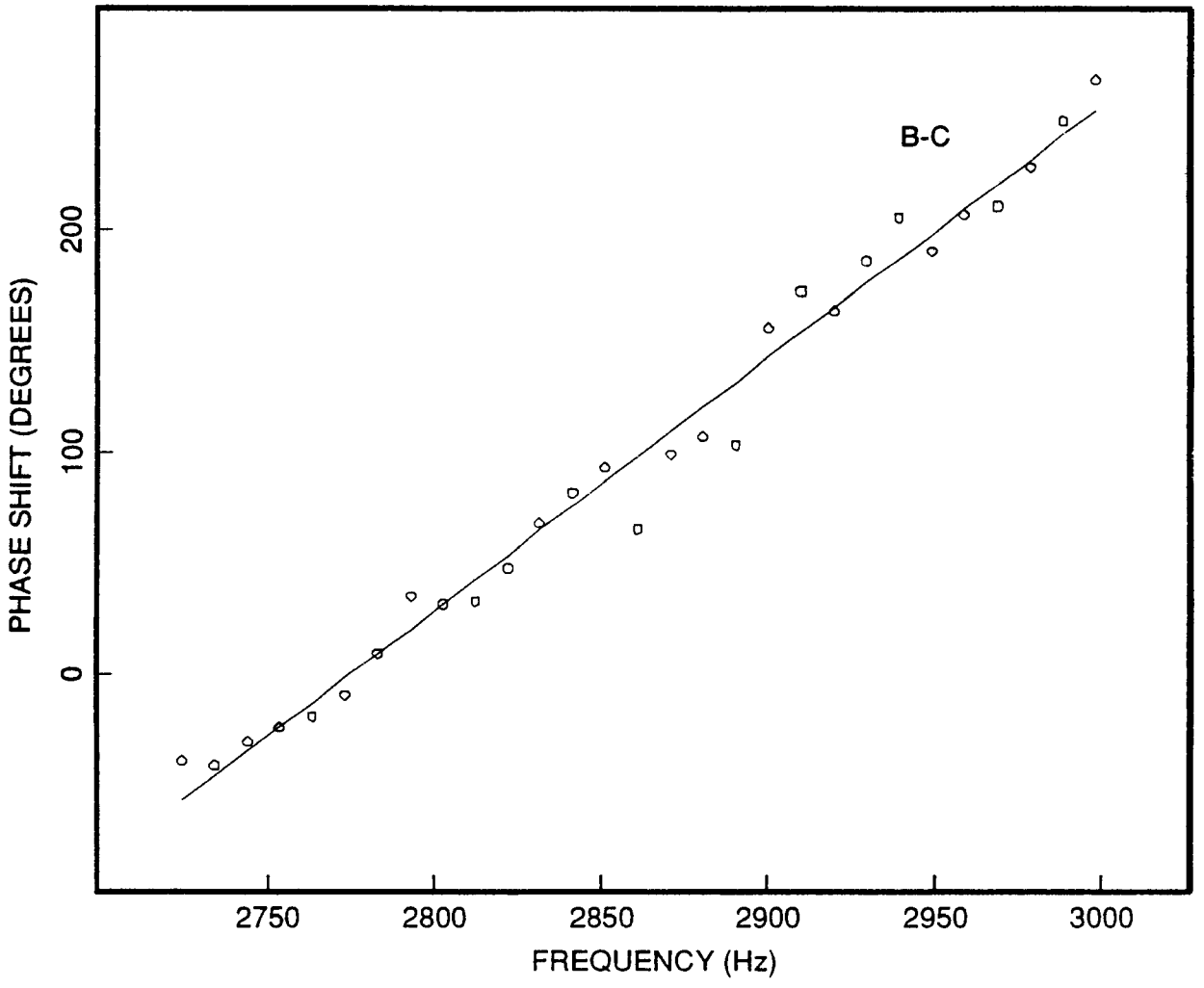

Figure 8.2. Unwrapped coherence phase between 2.7 and 3.0 kHz for sensor pair B-C of Figure 5.1 in which CO_2 is used as the product. The line pressure is 103 kPa (15 psi); the hole diameter is 0.7 mm. The estimated propagation speed (2400 m/s) is consistent with the nominal speed of transverse waves in steel.

The effect of multi-path and multi-mode wave propagation can also be observed in the coherence phase. Figure 8.3 shows a plot of the phase shift between sensors B and C in which the linear trend has been removed. The residual phase shift is dominated by a non-random, peri-

odic oscillation that occurs at approximately 50-Hz intervals with an average amplitude of 40°. If the signal received at each sensor is represented as a summation of a direct-path signal propagating at the observed wave speed and contaminating signals caused by multi-path and multi-mode propagation, an estimate can be made of the fraction of total energy received via the contaminating signals. A simple simulation in which approximately 15% of the total received energy was propagated by multi-path and multi-mode waves produced residual phase shifts comparable to those observed in the data.

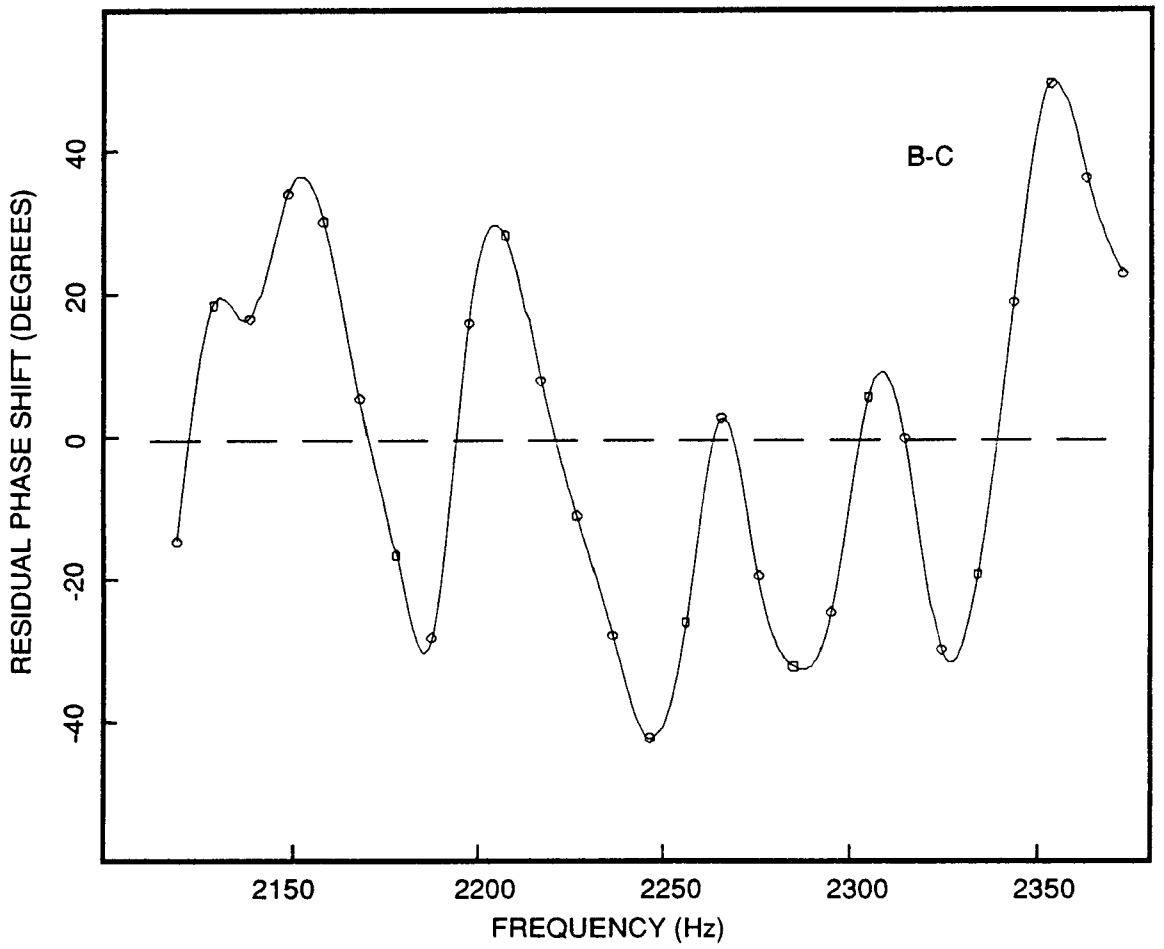

Figure 8.3. Unwrapped coherence phase between 2.1 and 2.4 kHz for sensor pair B-C in which the linear trend has been removed. The flow rate is 11.4 L/h (3 gal/h).

SECTION 9

PHASE UNWRAPPING

Accurate source location requires that the location algorithm distinguish between the information provided by the leak signal, and ambient or system noise. The continuous nature of the acoustic leak signal further requires that the separation of signal from noise take place in the frequency domain, through coherence function analysis, rather than in the time domain. It has been demonstrated that source location through cross-correlation analysis is not accurate when applied to wide frequency bands (e.g., the 1- to 4-kHz frequency band used in Figure 7.2). While the location estimates given in Table 7.1 are based upon the successful application of coherence function analysis to relatively narrow frequency bands (100 to 500 Hz), the possibility exists that a similar location algorithm may be applied to frequency bands of arbitrary wi dth.

Information concerning the leak location is contained in the coherence phase. Because the measured phase differs from the actual phase shift by an unknown multiple of 360°, the derivative of the coherence phase with respect to frequency, $d\phi/df$, is required in order to estimate the relative arrival time of leak signals at spatially separated sensor locations. When the relative separation between a pair of sensors is large compared to the wavelength of the received signals, some form of phase-unwrapping algorithm must be applied in order to measure $d\phi/df$ over a wide range of frequencies. Such unwrapping algorithms are easily implemented, provided that the coherence phase is reliably measured (i.e., the coherence amplitude is high) at many frequencies within the desired band. As the distribution of reliable phase estimates within a frequency band becomes more sparse, the ability to simply unwrap the phase is diminished, and the information provided by the phase measurements must be discarded. If the leak location and propagation speed of acoustic waves are known, the correspondence between measured and predicted phase shifts can be viewed over an arbitrarily wide frequency band.

Figures 9.1 and 9.2 show the unwrapped phase shift between sensors A-B, A-C, and B-C in which the unknown multiples of 360° required to unwrap the phase were computed from the predicted $\phi(f)$ lines (shown as solid lines in the figure). Reliable phase measurements (indicated by markers in the plots) correspond to coherence amplitudes that exceed the 95% level of statistical significance; the flow rates are 11.4 L/h (3 gal/h) (Figure 9.1) and 5.7 L/h (1.5 gal/h) (Figure 9.2). The frequency distribution of reliable phase measurements for the 11.4-L/h (3-gal/h) data is such that all of the information contained in the 2- to 4-kHz band can be used in

the location estimate by implementing a straightforward phase-unwrapping algorithm. As the flow rate is reduced, however, the simple unwrapping algorithm works only within a small number of narrow frequency bands (e.g., 2.2 to 2.5 kHz, and 3.7 to 4.0 kHz in Figure 9.2). The similarity between the measured and predicted phase shift outside of these narrow bands suggests that a more robust unwrapping algorithm may be capable of exploiting a greater fraction of the available phase information for the purpose of leak location.

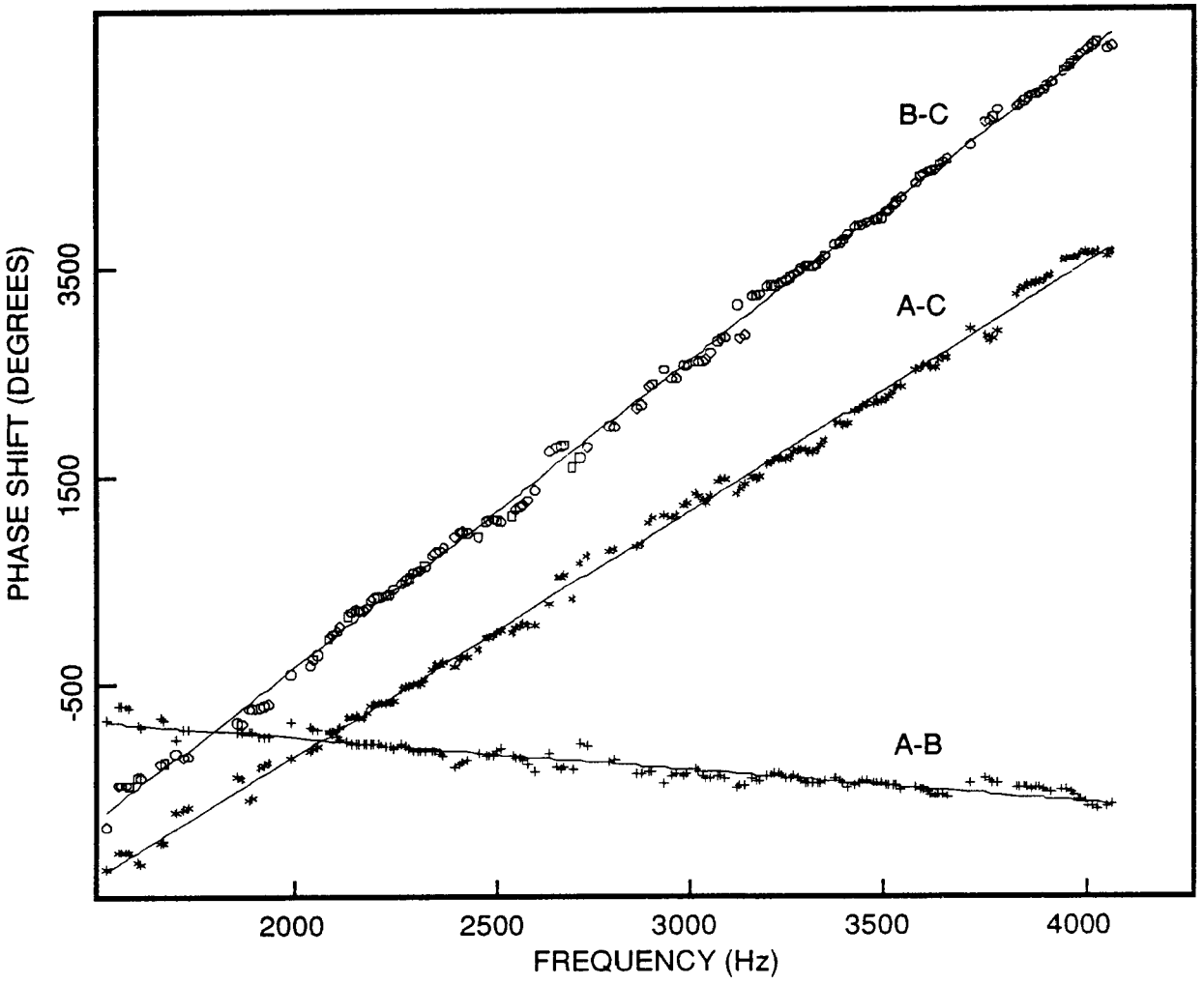

Figure 9.1. Unwrapped coherence phase between 1.5 and 4.5 kHz for sensor pairs A-B, A-C, and B-C. Solid lines indicate predicted coherence phase for linearly propagating plane waves based upon known leak location and propagation speed. Flow rate is 11.4 L/h (3 gal/h).

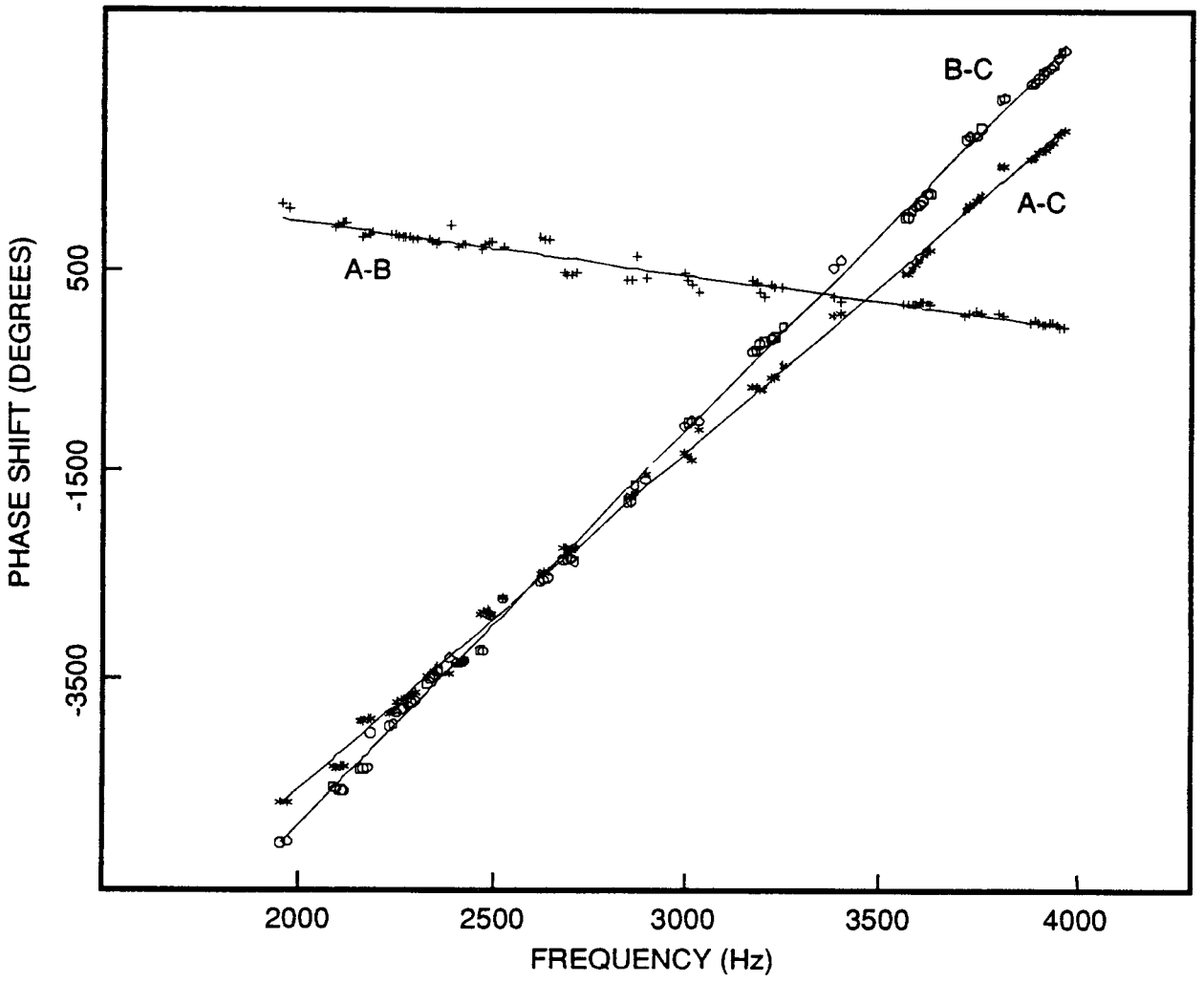

Figure 9.2. Unwrapped coherence phase between 1.5 and 4.5 kHz for sensor pairs A-B, A-C, and B-C. Solid lines indicate predicted coherence phase for linearly propagating plane waves based upon known leak location and propagation speed. Flow rate is 5.7 L/h (1.5 gal/h).

SECTION 10

REFERENCES

1. U.S. Environmental Protection Agency, "40 CFR 280 -- Technical Standards and Corrective Action Requirements for Owners and Operators of Underground Storage Tanks," *Federal Register*, Vol. 53, No. 185 (23 September 1988).
2. D. S. Kupperman, T. N. Claytor, T. Mathieson, and D. Prine, "Leak Detection Technology for Reactor Primary Systems," *Nuclear Safety*, Vol. 28 (April-June 1987).
3. D. S. Kupperman and D. E. Karvelas, "Acoustic Leak Detection for District Heating Systems," Technical Report No. ANL-87-60, Argonne National Laboratory, Argonne, Illinois (February 1988).
4. E. G. Eckert, J. W. Maresca, Jr., R. W. Hillger, and J. J. Yezzi, "Location of Leaks in Pressurized Pipelines by Means of Passive-Acoustic Sensing Methods," *Leak Detection Monitoring for Underground Storage Tanks, ASTM STP 1161*, Philip B. Durgin and Thomas M. Young, Eds., (Philadelphia: American Society for Testing and Materials, 1992).
5. J. S. Bendat and A. G. Piersol, *Engineering Applications of Correlation and Spectral Analysis* (New York: John Wiley & Sons, 1980).
6. R. J. Urick, *Principles of Underwater Sound* (New York: McGraw-Hill Book Company, 1967).
7. P. R. Roth, "Effective Measurements Using Digital Signal Analysis," *IEEE Spectrum*, Vol. 8 (April 1971).
8. J. W. Maresca, Jr., and R. H. Nakata, "Quality Assurance Project Plan: Remediation of Leaks in Underground Pressurized Pipeline Systems," Vista Research Project 1036, Vista Research, Inc., Mountain View, California (August 1991).
9. E. G. Eckert, and J. W. Maresca, Jr., "Detection of Leaks in the Floor of Aboveground Storage Tanks by Means of a Passive Acoustic Sensing System," *Proceedings of the 84th Annual Meeting and Exhibition of the Air and Waste Management Association*, Vancouver, British Columbia (1991).
10. E. G. Eckert and J. W. Maresca, Jr., "Field Tests of Passive Acoustic Leak Detection Systems for Aboveground Storage Tanks When In Service," *Proceedings of the 85th Annual Meeting and Exhibition of the Air and Waste Management Association*, Kansas City, Missouri (1992).
11. E. G. Eckert and J. W. Maresca, Jr., "An Engineering Assessment of Acoustic Methods of Leak Detection in Aboveground Storage Tanks," Final Report for API, Vista Research, Inc., Mountain View, California (October 1991).

TECHNICAL REPORT DATA
(Please read Instructions on the reverse before completing)

1. REPORT NO.	2.	3. RECIPIENT'S ACCESSION NO.
EPA/600/R-92/143		PB92-207 687

4. TITLE AND SUBTITLE	5. REPORT DATE
ACOUSTIC LOCATION OF LEAKS IN PRESSURIZED UNDERGROUND PETROLEUM PEPELINES	August 1992
	6. PERFORMING ORGANIZATION CODE

7. AUTHOR(S)	8. PERFORMING ORGANIZATION REPORT NO.
Eric G. Eckert and Joseph W. Maresca, Jr. Vista Research, Inc., Mountain View, CA 94042	

9. PERFORMING ORGANIZATION NAME AND ADDRESS	10. PROGRAM ELEMENT NO.
CDM Federal Programs Corporation 13135 Lee Jackson Memorial Highway - Suite 200 Fairfax, Virginia 22033	CBRD1A
	11. CONTRACT/GRANT NO. 68-03-3409

12. SPONSORING AGENCY NAME AND ADDRESS	13. TYPE OF REPORT AND PERIOD COVERED
Risk Reduction Engineering Laboratory--Cin., OH Office of Research and Development US Environmental Protection Agency Cincinnati, Ohio 45268	Project Report
	14. SPONSORING AGENCY CODE EPA 600/14

15. SUPPLEMENTARY NOTES

Project Officer: Robert W. Hillger (FTS) 340-6639 Comm: (908) 321-6603

16. ABSTRACT

Experiments were conducted at the UST Test Apparatus Pipeline in which three acoustic sensors separated by a maximum distance of 38 m (125-ft) were used to monitor signals produced by 3.0-, 1.5-, and 1.0-gal/h leaks in the wall of a 2-in.-diameter pressurized petroleum pipeline. The range of line pressures and hole diameters used in the experiments were 10 to 20 psi, and 0.4 to 0.7 mm, respectively. Application of a leak location algorithm based upon the technique of coherence function analysis resulted in mean differences between predicted and actual leak locations of approximately 10 cm. The standard deviations of the location estimates were approximately 30 cm. This is a significant improvement (i.e., smaller leaks over longer distances) over the cross-correlation-based techniques, which are currently being used. Spectra computed from leak-on and leak-off time series indicate that the majority of acoustic energy received in the far-field of the leak is concentrated in a frequency band from 1 to 4 kHz. The strength of the signal within this band was found to be proportional to the leak flow rate and line pressure. Energy propagation from leak to sensor was observed via three types of wave motion: longitudinal waves in the product, and longitudinal and transverse waves in the steel. The similarity between the measured wave speed and the nominal speed of sound in gasoline suggests that longitudinal waves in the product dominate the spectrum of received acoustic energy. The effects of multiple-mode wave propagation and the reflection of acoustic signals within the pipeline were observed as non-random fluctuations in the measured phase difference between sensor pairs. Additional experiments with smaller holes and higher pressures (20 to 50 psi) are required to determine the smallest leaks that can be located over distances of several hundred feet. The current experiments indicate that improved phase-unwrapping algorithms and/or lower noise instrumentation are required to optimize system performance. This report was submitted in fulfillment of Contract No. 68-03-3409 by Vista Research, Inc., under the sponsorship of the U.S. Environmental Protection Agency. This report covers a period from 23 January 1991 to 31 October 1991, and work was completed as of 30 September 1991.

17. KEY WORDS AND DOCUMENT ANALYSIS

a. DESCRIPTORS	b. IDENTIFIERS/OPEN ENDED TERMS	c. COSATI Field/Group
Detection Pipeline Petroleum Gasoline Acoustic	UST Underground Storage Tanks Leak	

18. DISTRIBUTION STATEMENT	19. SECURITY CLASS *(This Report)*	21. NO. OF PAGES
Release to Public	Unclassified	57
	20. SECURITY CLASS *(This page)*	22. PRICE
	Unclassified	

EPA Form 2220-1 (9-73)

☆U.S. GOVERNMENT PRINTING OFFICE: 1992 - 648-003/60010